Computational Design and Performance Prediction of Creep-Resistant Ferritic Superalloys

FE0024054

Investigators: Peter K. Liaw[1], David C. Dunand[2], and Gautam Ghosh[2]

Students: Gian Song[1], Michael Rawings[2], Shao-Yu Wang[1], and Zhiqian Sun[1]

[1]The University of Tennessee, Knoxville (UTK)

[2]Northwestern University (NU)

U.S. Department of Energy
National Energy Technology Laboratory
Strategic Center for Coal

Acknowledgements

We are very grateful to:

(1) Richard Dunst
(2) Vito Cedro
(3) Patricia Rawls
(4) Robert Romanosky
(5) Susan Maley
(6) Regis Conrad
(7) Jessica Mullen
(8) Mark D. Asta
(9) Morris E. Fine
(10) C. T. Liu
(11) Nicholas Anderson, for their kind support and encouragement, and
(12) National Energy Technology Laboratory (NETL) for sponsoring this project

Outline

- Technical Background of the Project
  - Why NiAl/Ni_2TiAl-strengthened ferritic alloys
- Objectives
- Current Progress
  - First-Principles Calculations
  - Experimental Results
- Ongoing Research
- Future Plan
- Conclusions
- Papers and Presentations

Technical Background of the Project

Ni-based Superalloys

- Higher-temperature capability compared to other superalloys (austenitic and ferritic superalloys)
- Most-widely-used high-temperature materials

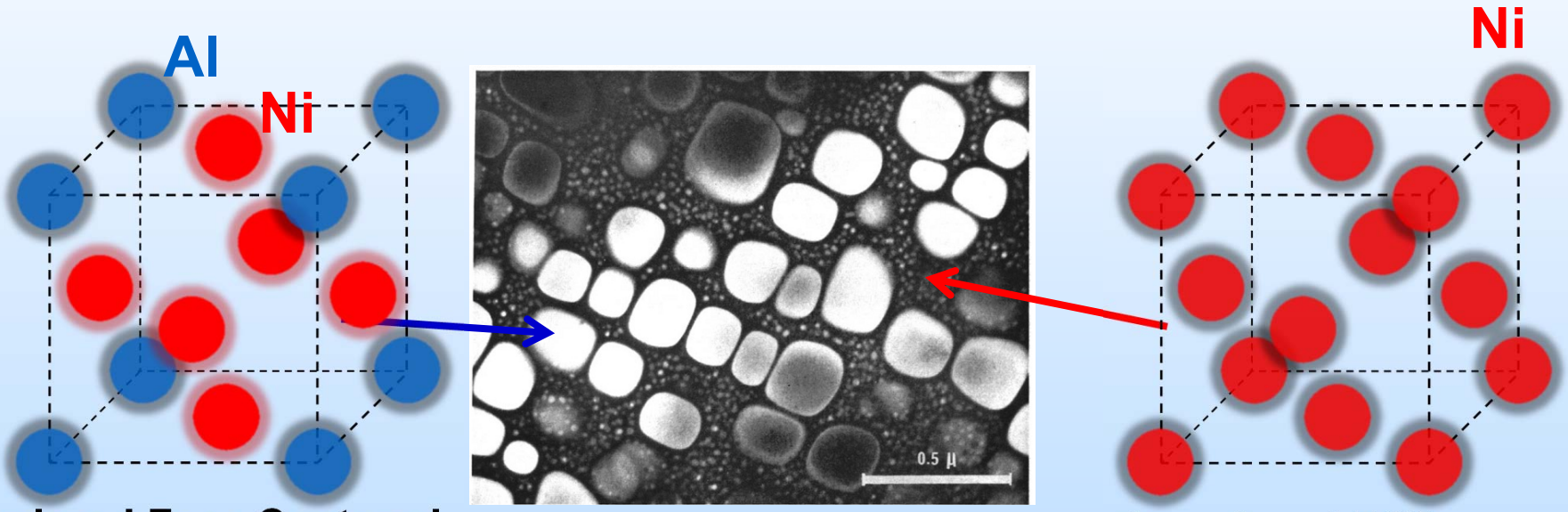

Ordered Face Centered Cubic (FCC) structure (Ni_3Al: $L1_2$)

Disordered FCC structure

Dark-field thin-foil micrograph of Udimet-700 alloy [Ni-15Co-15Cr-5Mo-3.5Fe-4.3Al-3.5Ti-0.05C, in weight percent]
P.S, Kotval, Metallography, 1, 251 (1969)

NiAl-hardened Ferritic Superalloys

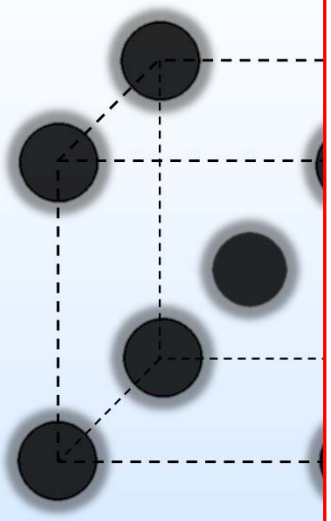

Fe (a phas

a = 0.28665

Similar lattice s

Ni-based super

Larson-Miller diagram

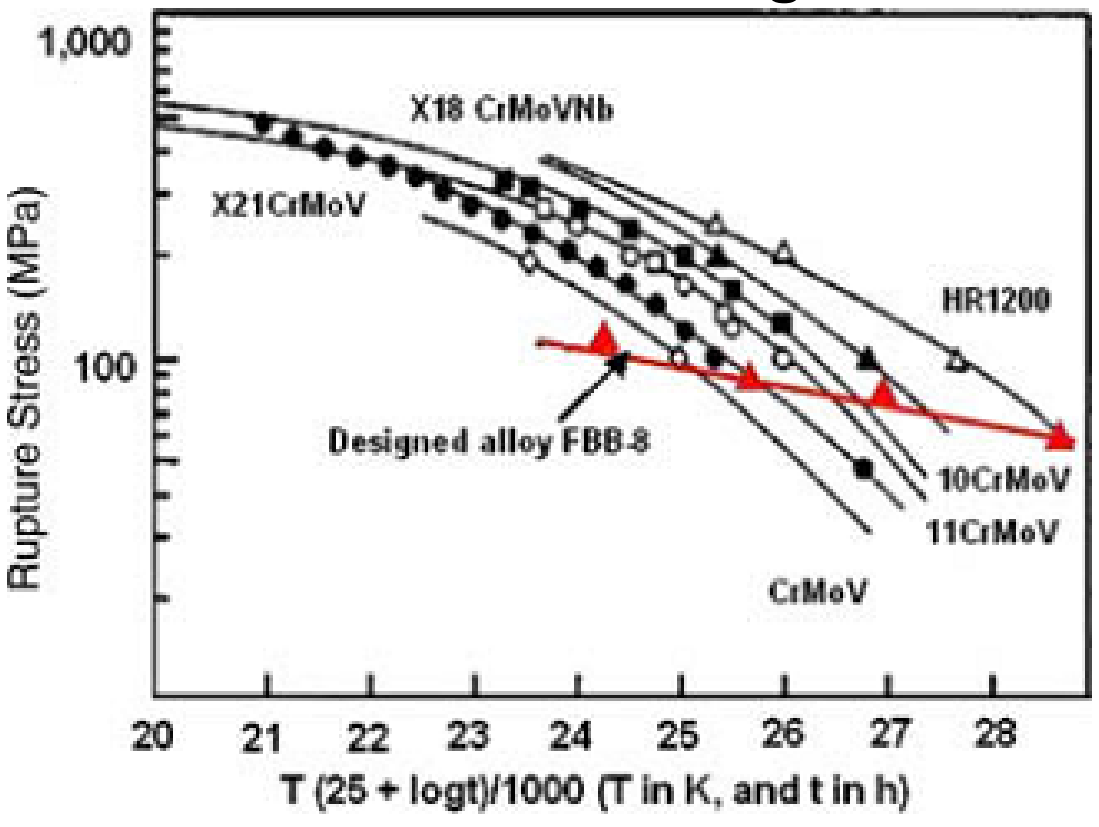

38

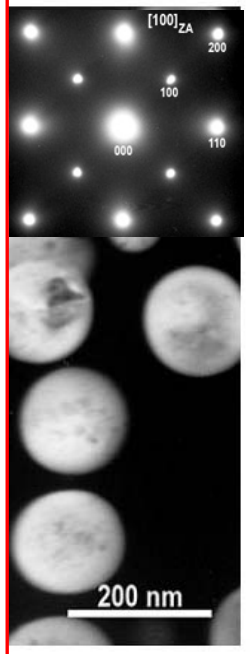

→ analogue to

At high stresses (> 100 MPa) → inferior creep resistance compared to other Fe-based materials candidates for steam-turbine applications

However….

1) S. Huang, D. Brown, B. Clausen, Z. Teng, Y. Gao, P.K. Liaw, Metallurgical and Materials Transactions A, 43 (2011) 1497-1508.

2) S. Huang, Y. Gao, K. An, L. Zheng, W. Wu, Z. Teng, P.K. Liaw, Acta Mater., 83 (2015) 137-148.

$L2_1$-Ni_2TiAl Structure Phase as a New Precipitate

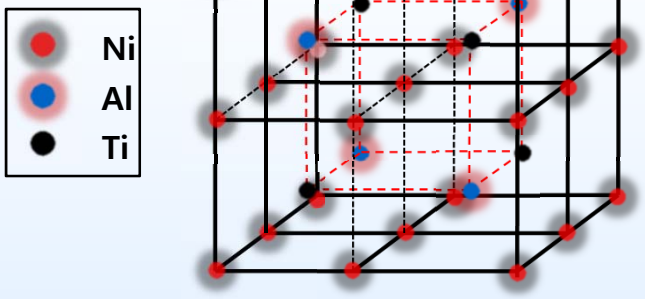

Ni_2TiAl ($L2_1$)
α/2 = 0.29325 nm

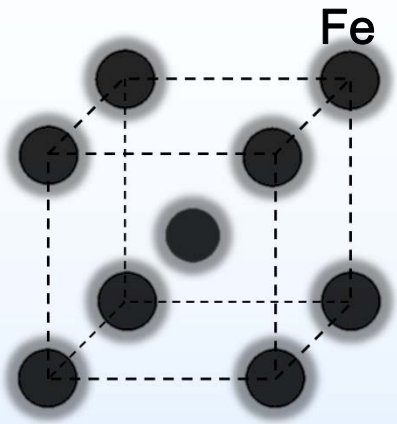

Fe (α phase)
a = 0.28665 nm

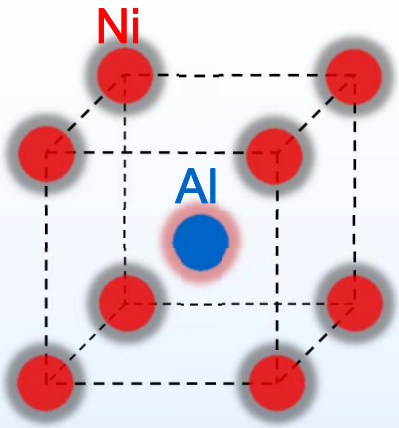

NiAl (B2 phase)
a = 0.28864 nm

The small cells constituting the large Ni_2AlTi unit cell are 1.7 % larger in size than the NiAl unit cell

1) P. Strutt, R. Polvani, J. Ingram, Metallurgical and Materials Transactions A, 7 (1976) 23-31
2) R. Polvani, W.-S. Tzeng, P. Strutt, Metallurgical and Materials Transactions A, 7 (1976) 33-40.

- The elevated-temperature strength of NiAl-type (B2) precipitates is limited by their properties.
- The creep strength of Ni_2TiAl ($L2_1$) between 1,026 and 1,273 K is about three times that of NiAl in its most creep-resistant form.
- The creep strength of NiAl-Ni_2TiAl two-phase alloys are more creep resistant than either of the phases in its monolithic form and at least comparable to the Ni-based superalloy, MAR-M200 (nominal composition wt.%: Cr 9.0; Co 10.0; W 12.5; Nb 1.0; Ti 2.0; Al 5.0; C 0.15; B 0.015; Ni balance).

Hypothesis: $L2_1$-Structure Phase as a New Precipitate

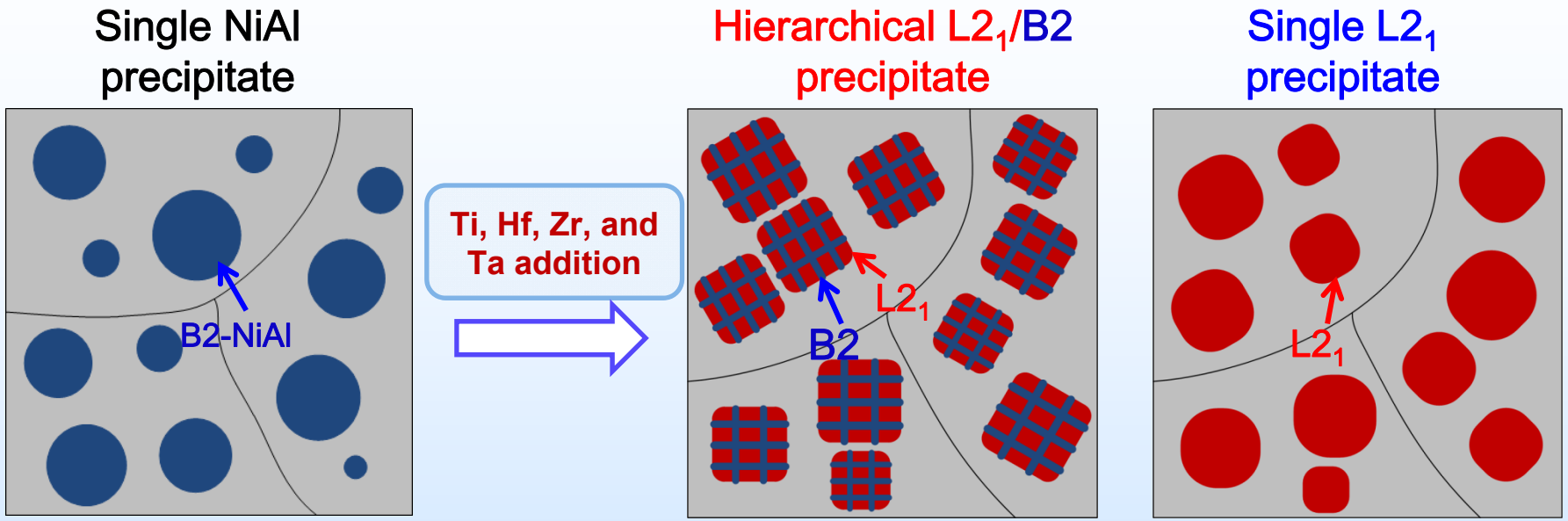

FBB8: Fe-6.5Al-10Cr-10Ni-3.4Mo-0.25Zr-0.005B, weight percent (wt.%): FBB8

Novel Precipitate Structures

Effect of precipitate structures on creep properties (hierarchical B2/$L2_1$ and single $L2_1$ structure)

What are critical parameters for creep resistance? (volume/size/morphology)

Objectives

- **Objective 1:** To develop and integrate modern computational tools and algorithms, i.e., predictive first-principles calculations, computational-thermodynamic modeling, and meso-scale dislocation-dynamics simulations, to design high-temperature alloys for applications in fossil energy power plants.

- **Objective 2:** To understand the processing-microstructure-property-performance links underlying the creep behavior of novel ferritic alloys strengthened by hierarchical coherent B2/$L2_1$ precipitates.

Schematic Illustration of Current Study

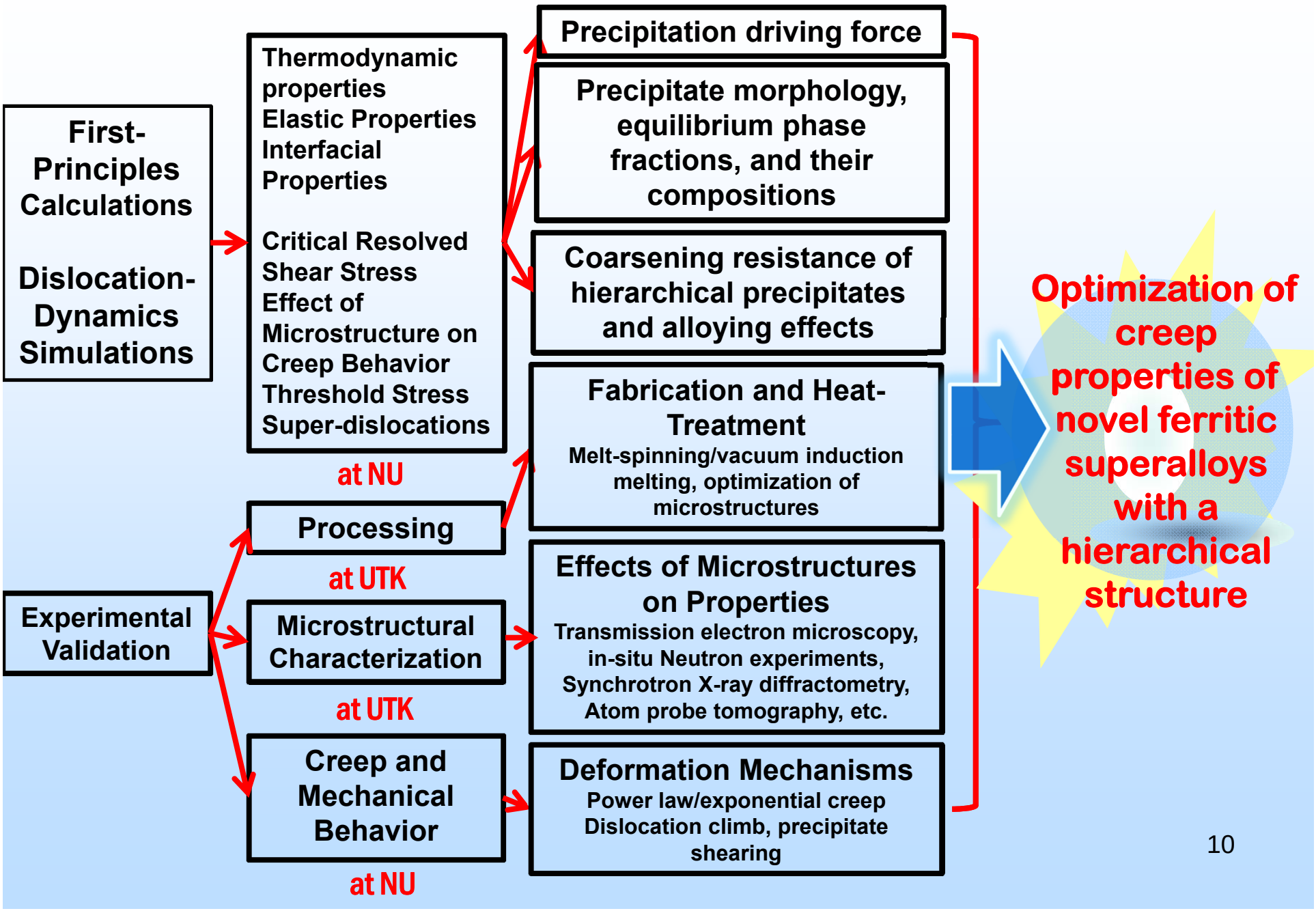

Current Progress

First-Principles Calculations

Calculations of Elastic Constants of Fe, *B*2, and $L2_1$ Phases

$$E(V,\{e_i\}) = E(V_0,0) - PV_0\sum_{i=1}^{3} e_i + \frac{V_0}{2}\sum_{i=1}^{6}\sum_{j=1}^{6} C_{ij} e_i e_j + O[e_i^3]$$

E: internal energy
e_i: infinitesimal strain
V_0: volume of the unstrained crystal
C_{ij}: single-crystal elastic constants
P: pressure of the undistorted crystal at a volume, V_0

- **Heusler Phases (in GPa)**

Elastic Constant \ Phase	Ni_2TiAl	Fe_2TiAl	Co_2TiAl
C_{11}	211.87	313.75	288.89
C_{12}	143.39	124.07	137.79
C_{44}	87.23	108.77	111.88

- **C_{ij}s are obtained by a first-principles method: total energy of the system, $E(V,\{e_i\})$, as a function of deformation.**
- **There is NO experimental C_{ij} data of Heusler phases. Thus, calculations from first-principles is the only viable option.**
- **C_{ij} is needed to understand the morphology of coherent precipitates and interfacial energy.**

Experimental Results

TEM Microstructural Characterization on 4% Ti Alloy

Fe-4Ti-6.5Al-10Cr-10Ni-3.4Mo-0.25Zr-0.005B (wt. %), aged at 973 K for 100 hs

<110> zone axis diffraction pattern

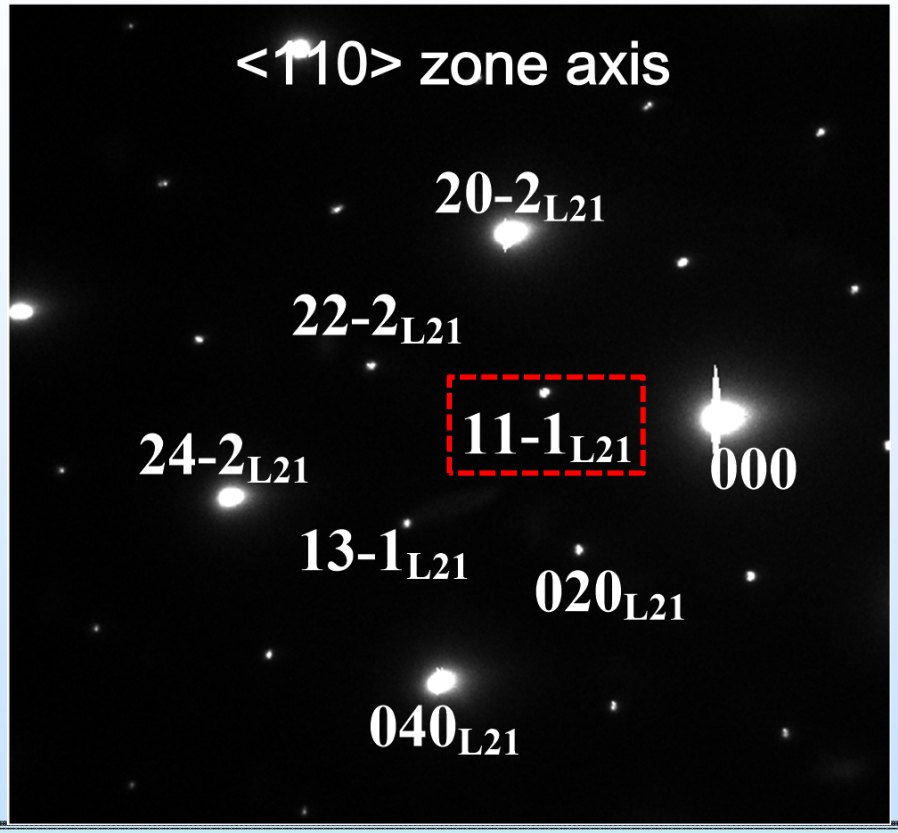

Dark-field (DF) image using <111>

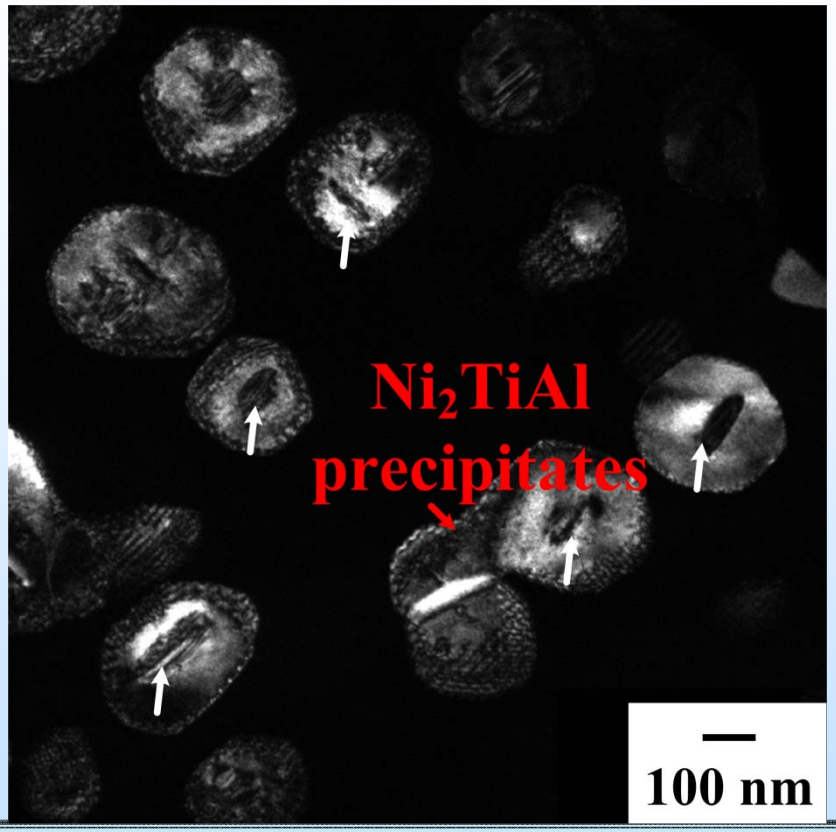

- **Formation of $L2_1$-Ni_2TiAl precipitates**
- **A network of misfit dislocations is present at the precipitate-matrix interface→ higher misfit between the Fe and $L2_1$ phases**

G. Song, Z. Q. Sun, L. Li, X. D. Xu, M. Rawlings, C. H. Liebscher, B. Clausen, J. Poplawsky, D. N. Leonard, S. Y. Huang, Z. K. Teng, C. T. Liu, M. D. Asta, Y. F. Gao, D. C. Dunand, G. Ghosh, M. W. Chen, M. E. Fine, and P. K. Liaw, Scientific Reports, Vol. 5, p. 16327 (2015)

TEM Microstructural Characterization on 2% Ti Alloy

Fe-2Ti-6.5Al-10Cr-10Ni-3.4Mo-0.25Zr-0.005B (wt. %), aged at 973 K for 100 hs

<100> zone axis diffraction pattern

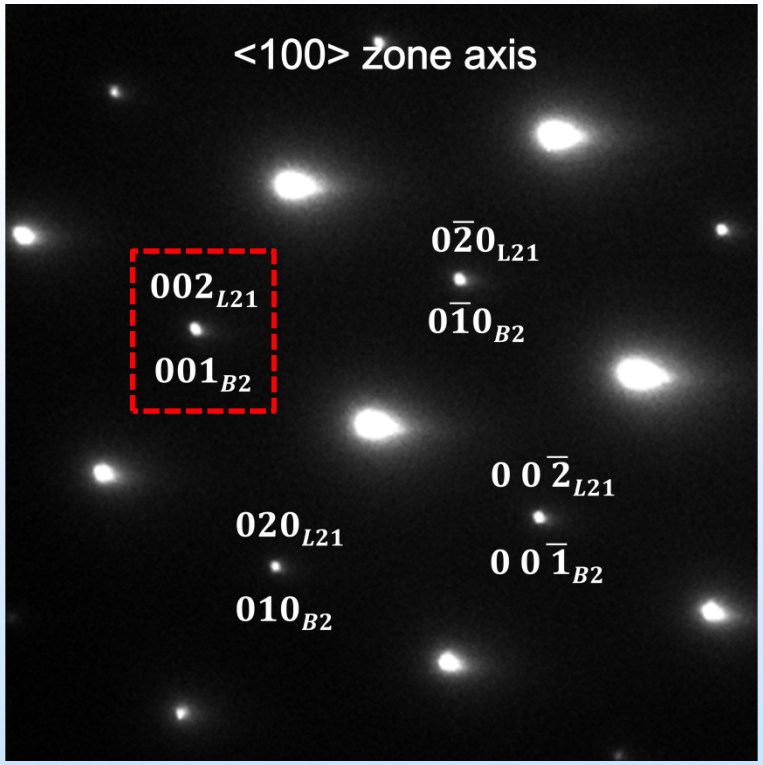

Dark-field (DF) image using <001>

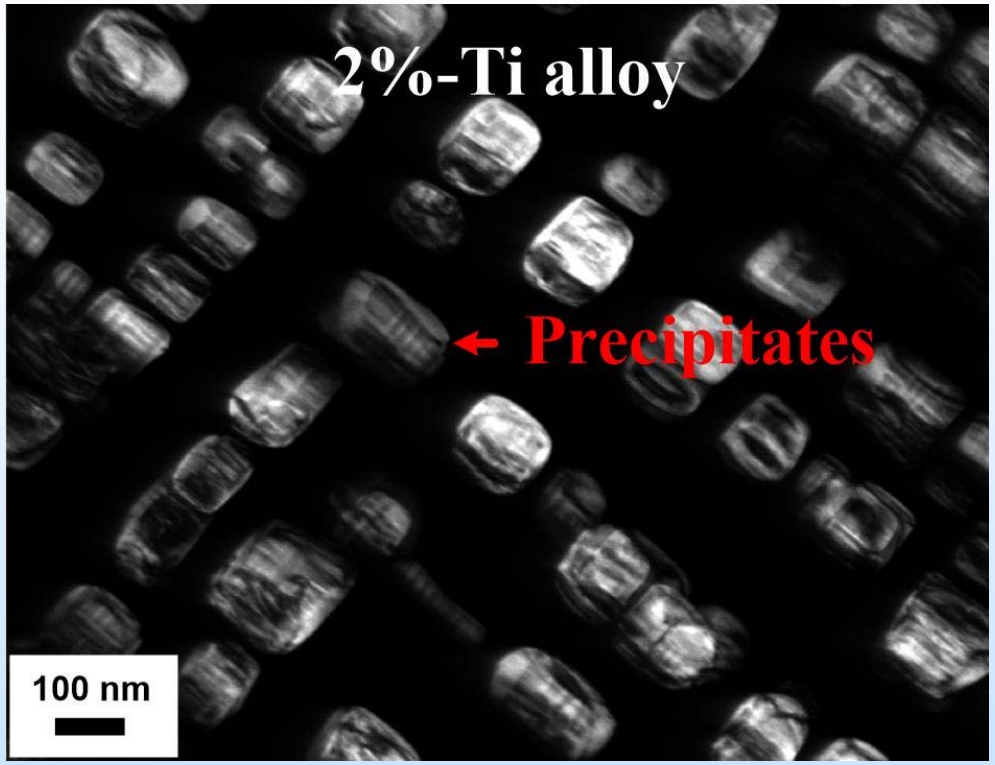

- Overlapping of the superlattice peaks between the $L2_1$ and B2 structures in the <100> direction
- Coherent cuboidal precipitates (no interface dislocation)
- Internal structure inside the precipitates → presence of second phase

G. Song, Z. Q. Sun, L. Li, X. D. Xu, M. Rawlings, C. H. Liebscher, B. Clausen, J. Poplawsky, D. N. Leonard, S. Y. Huang, Z. K. Teng, C. T. Liu, M. D. Asta, Y. F. Gao, D. C. Dunand, G. Ghosh, M. W. Chen, M. E. Fine, and P. K. Liaw, Scientific Reports, Vol. 5, p. 16327 (2015)

TEM Microstructural Characterization on 2% Ti Alloy (Cont'd)

Fe-2Ti-6.5Al-10Cr-10Ni-3.4Mo-0.25Zr-0.005B (wt. %), aged at 973 K for 100 hs

- Confirmation of B2-NiAl formation within $L2_1$-Ni_2TiAl parent precipitate

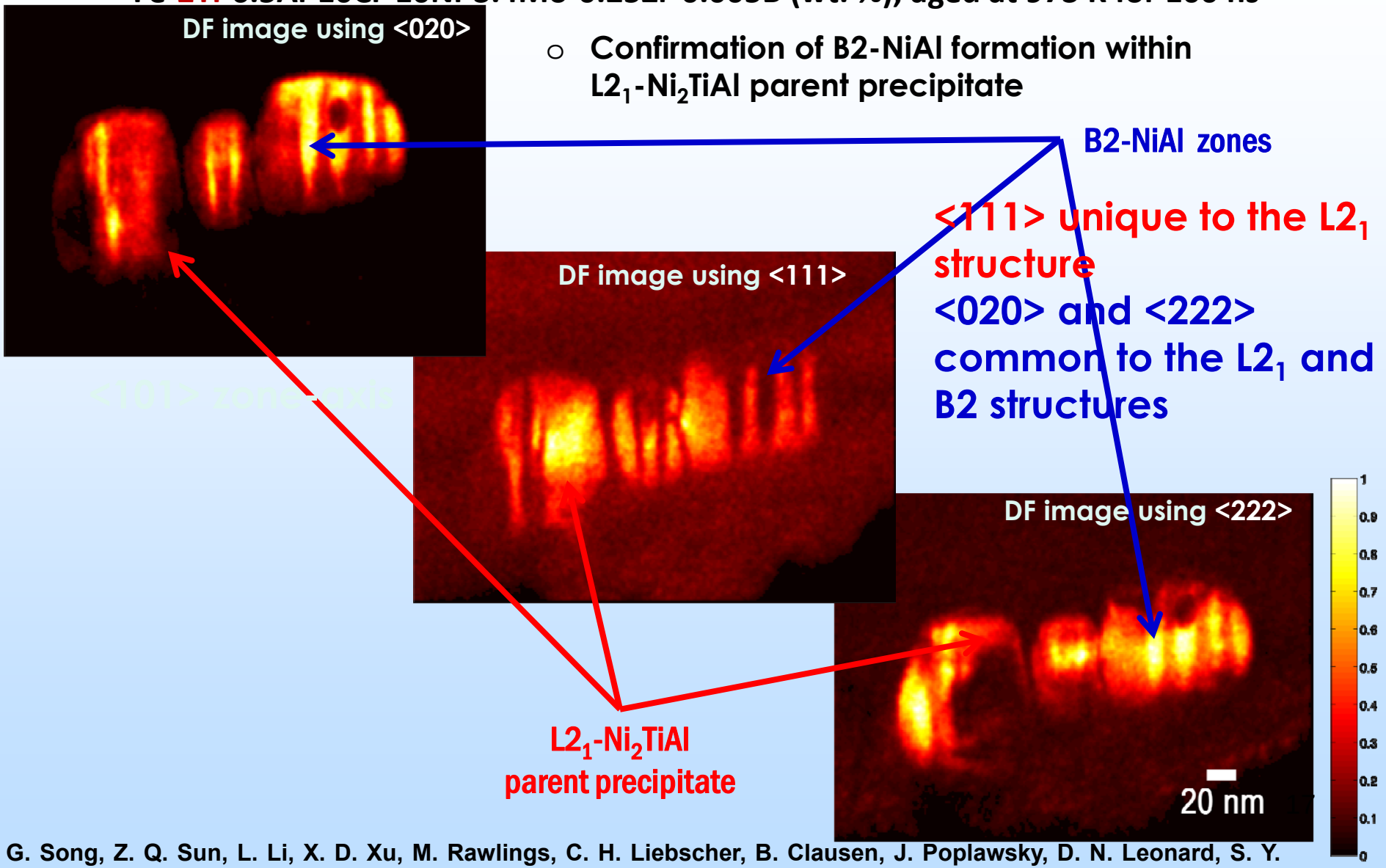

G. Song, Z. Q. Sun, L. Li, X. D. Xu, M. Rawlings, C. H. Liebscher, B. Clausen, J. Poplawsky, D. N. Leonard, S. Y. Huang, Z. K. Teng, C. T. Liu, M. D. Asta, Y. F. Gao, D. C. Dunand, G. Ghosh, M. W. Chen, M. E. Fine, and P. K. Liaw, Scientific Reports, Vol. 5, p. 16327 (2015)

Atom Probe Tomography on 2% Ti Alloy

Fe-2Ti-6.5Al-10Cr-10Ni-3.4Mo-0.25Zr-0.005B (wt. %), aged at 973 K for 100 hs

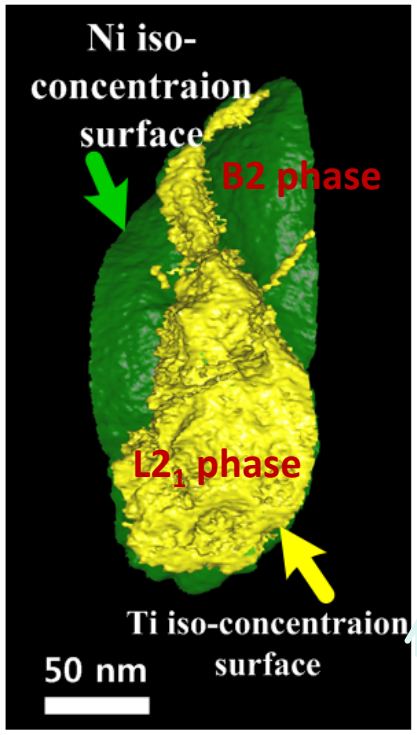

Center for Nano-phase Materials Sciences at ORNL (DOE)

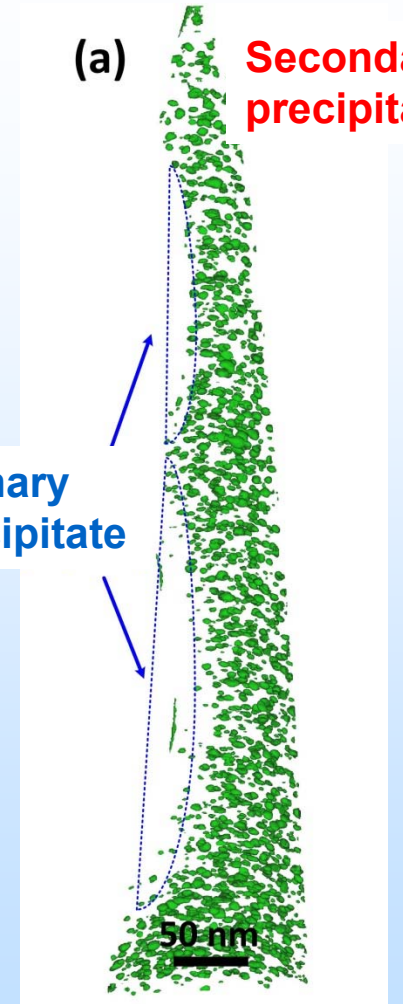

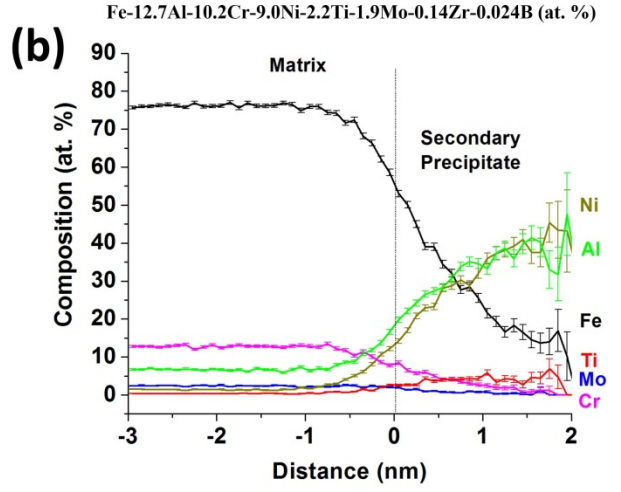

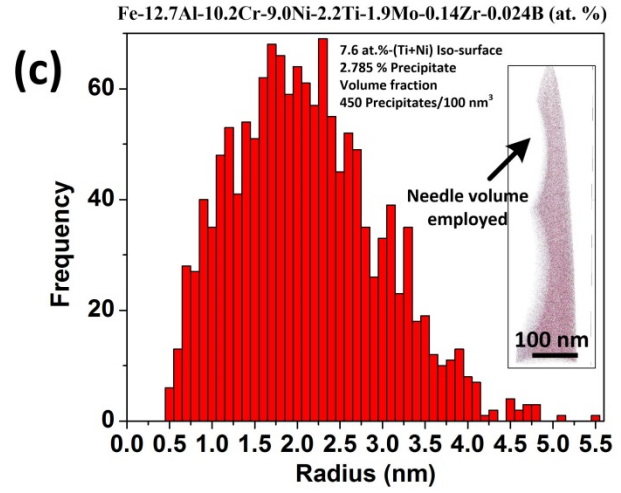

The presence of NiAl zones in the main $L2_1$ precipitate

Strong evidence of the hierarchical structure in the main precipitate

Formation of ultra-fine precipitates in the Fe matrix

G. Song, Z. Q. Sun, L. Li, X. D. Xu, M. Rawlings, C. H. Liebscher, B. Clausen, J. Poplawsky, D. N. Leonard, S. Y. Huang, Z. K. Teng, C. T. Liu, M. D. Asta, Y. F. Gao, D. C. Dunand, G. Ghosh, M. W. Chen, M. E. Fine, and P. K. Liaw, Scientific Reports, Vol. 5, p. 16327 (2015)

Creep Behavior (Cont'd)

Fe-6.5Al-10Cr-10Ni-3.4Mo-0~4Ti-0.25Zr-0.005B (wt.%)

Heat Treatment: Homogenized at 1200 °C for 0.5 h, then aged at 700 °C for 100 h

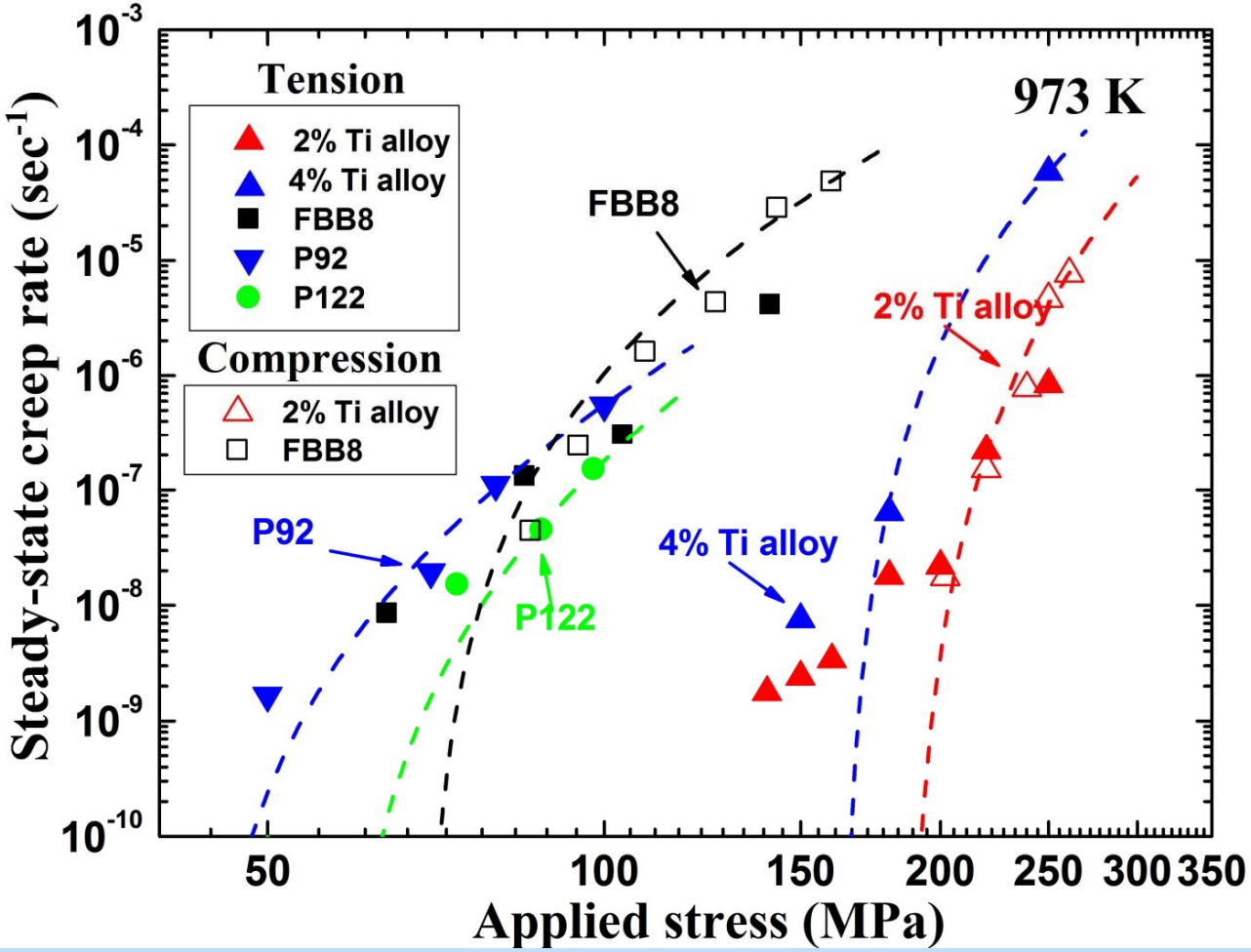

Steady-state creep rate vs applied stress of 0 (base alloy), 2 and 4 wt.% Ti alloys at 700 °C.

P92: Fe-9.09Cr-1.83W-0.61Mn-0.43Mo-0.23Si-0.21Ni-0.20V-0.10C-0.064Nb-0.046N-0.008P-0.003Al-0.0012B (wt. %)

P122: Fe-10.15Cr-1.94W-0.61Mn-0.36Mo-0.27Si-0.34Ni-0.20V-0.13C-0.055Nb-0.057N-0.014P-0.017Al-0.0019B (wt. %)

G. Song, Z. Q. Sun, L. Li, X. D. Xu, M. Rawlings, C. H. Liebscher, B. Clausen, J. Poplawsky, D. N. Leonard, S. Y. Huang, Z. K. Teng, C. T. Liu, M. D. Asta, Y. F. Gao, D. C. Dunand, G. Ghosh, M. W. Chen, M. E. Fine, and P. K. Liaw, Scientific Reports, Vol. 5, p. 16327 (2015)

Ongoing Research

Fe-1Ti-1Hf-6.5Al-10Cr-10Ni-3.4Mo-0.25Zr-0.005B (wt. %), Solution treatment at 1,200 °C for 0.5 hour, followed by aging treatment at 700 °C for 100 hours.

- The SEM image shows the presence of larger precipitates within grains and along the grain-boundaries.
- The TEM image shows that, there is B2 precipitates exist, but not the hierarchical structural precipitates.

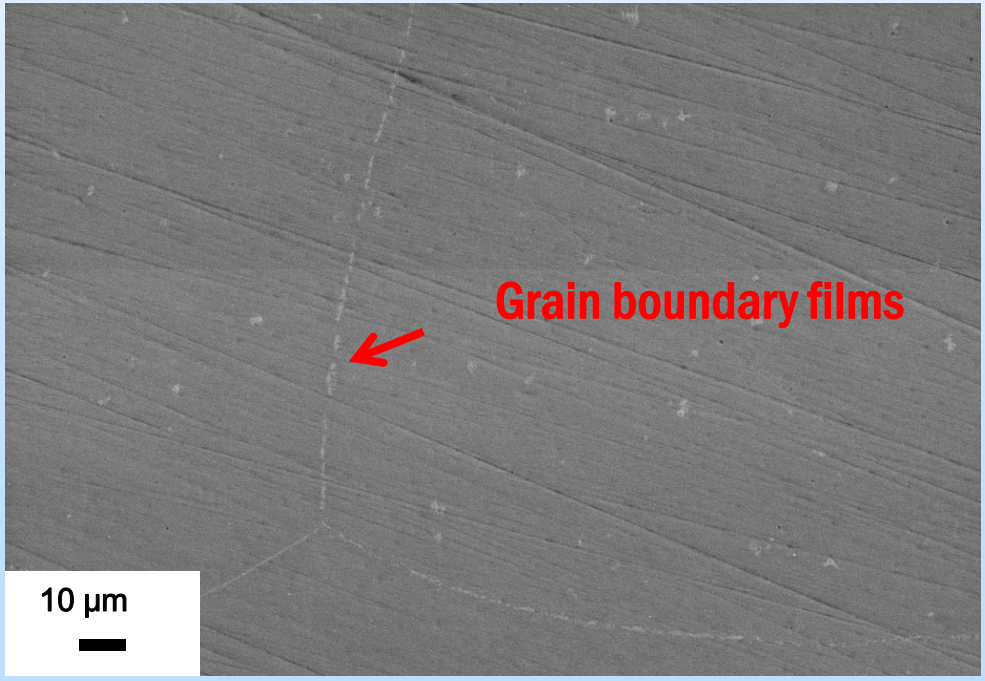

<110> zone axis diffraction pattern

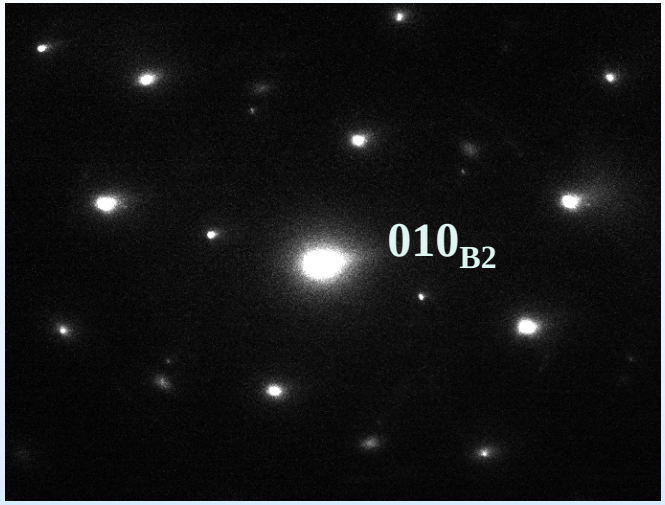

DF TEM image

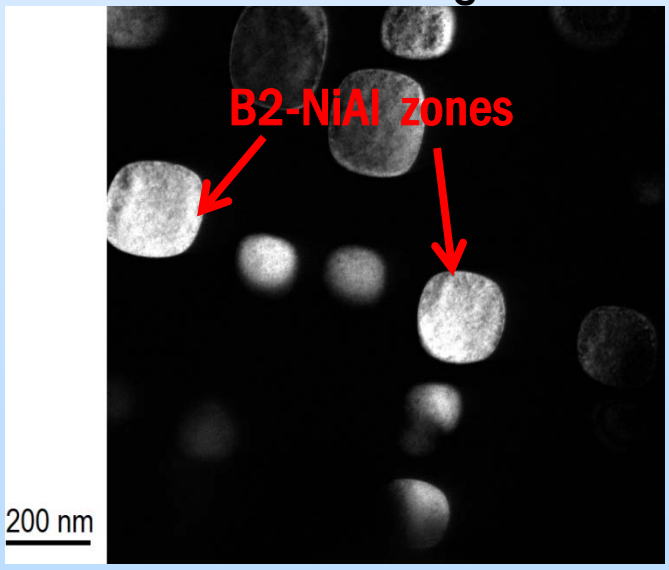

Fe-1Ti-1Hf-6.5Al-10Cr-10Ni-3.4Mo-0.25Zr-0.005B (wt. %), Solution treatment at 1,200 °C for 0.5 hour, followed by aging treatment at 700 °C for 100 hours (Cont'd)

High-angle Annular Dark-field (HAADF) TEM image

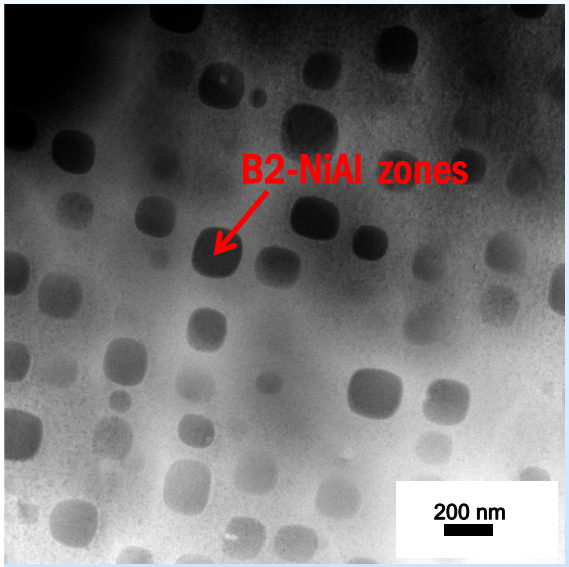

Energy Dispersive X-ray (EDX) spectroscopy mapping

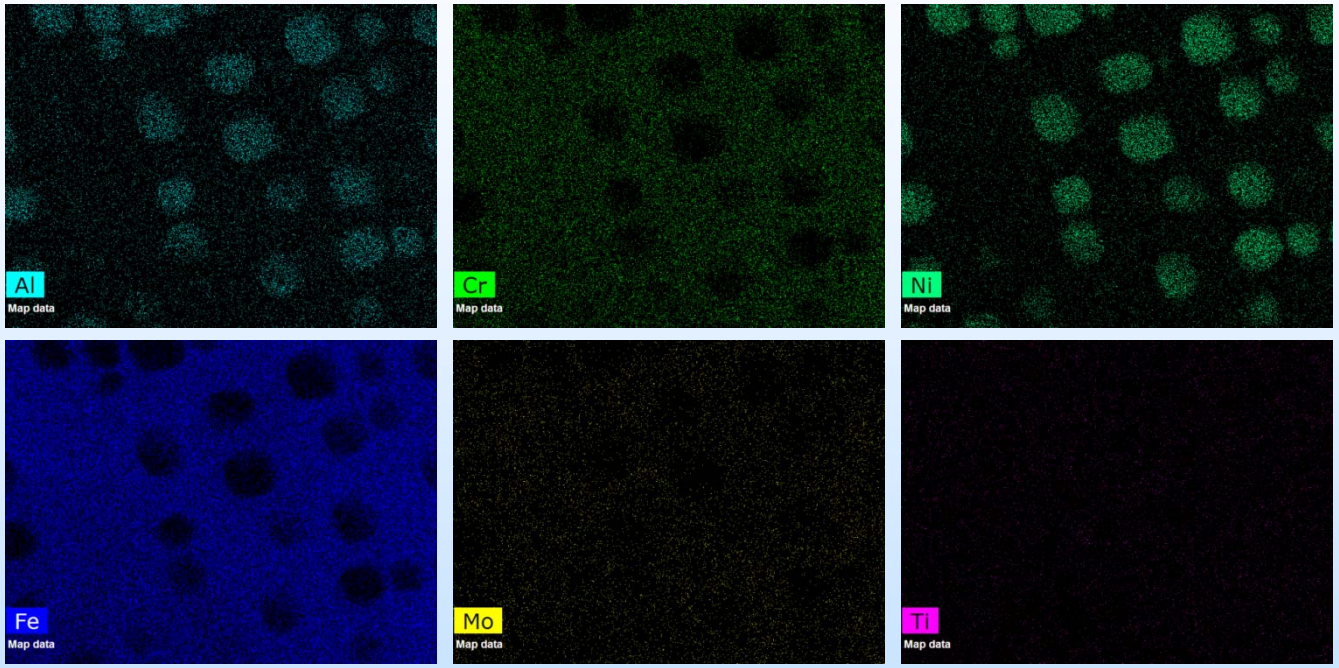

EDX results (at. %)

	Al	Ti	Cr	Fe	Ni	Zr	Mo	Hf
ppt	21.0 ± 0.07	1.8 ± 0.01	1.3 ± 0.03	17.9 ± 0.14	57.2 ± 0.23	0.2 ± 0.04	0.3 ± 0.08	0.3 ± 0.11
Matrix	5.2 ± 0.45	1.3 ± 0.05	12.4 ± 0.13	75.3 ± 0.76	3.3 ± 0.14	0.1 ± 0.05	2.2 ± 0.03	-

Fe-2Hf-6.5Al-10Cr-10Ni-3.4Mo-0.25Zr-0.005B (wt. %), Solution treatment at 1,200 °C for 0.5 hour, followed by aging treatment at 700 °C for 100 hours

- SEM on 2%-Hf alloy showed similar microstructure as 1%-Hf-1%-Ti alloy. Various of undesirable precipitates formed in the grains and along the grain boundaries.
- Three kinds of precipitate morphologies have been recognized. Spherical, cuboidal, and nano-sized precipitates.
- These undesirable precipitates are large. According to the calculation of dislocation-dynamics simulation, these μm-sized precipitates do not help the enhancement of creep strength.
- On the other hand, forming these larger size of precipitates consume the elements required for forming nano-sized hierarchical precipitates.

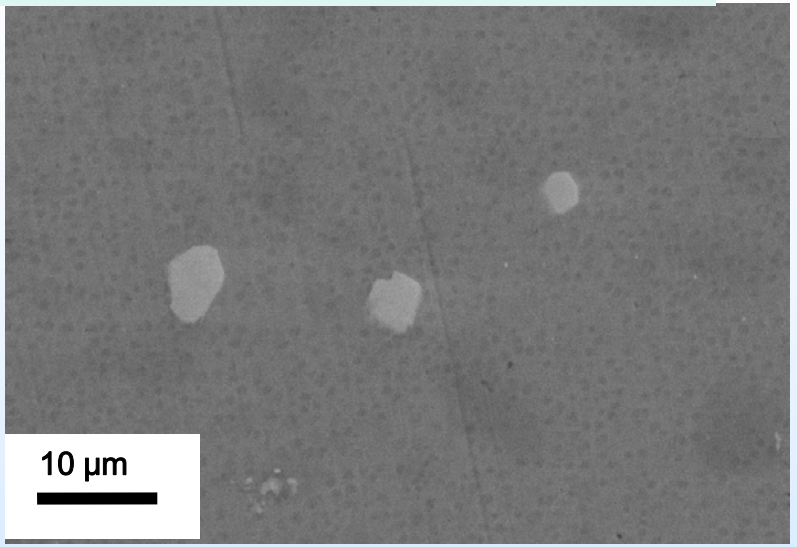

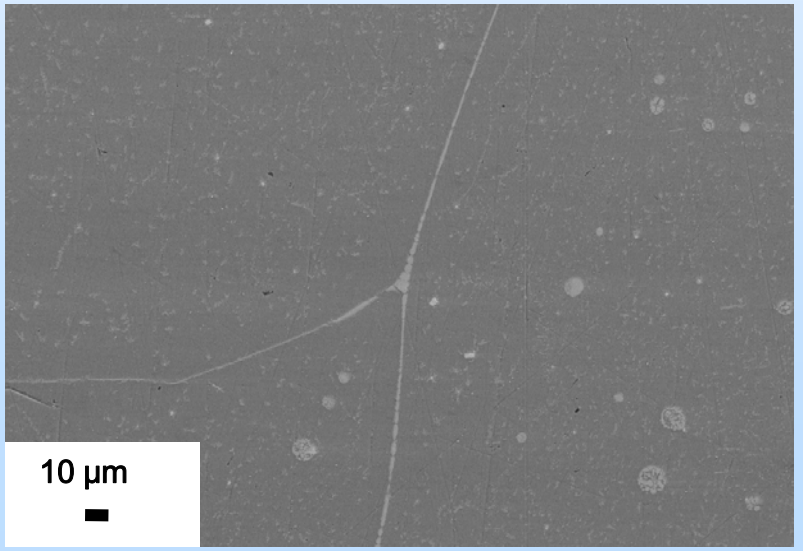

Fe-2Hf-6.5Al-10Cr-10Ni-3.4Mo-0.25Zr-0.005B (wt. %), Solution treatment at 1,200 °C for 0.5 hour, followed by aging treatment at 700 °C for various periods

- The 2%-Hf alloy was homogenized at 1,200 ˚C for 30 minutes, followed by air cooling and, then, aged at 700 ˚C for 24 hours, 44 hours, 68 hours, 84 hours, 108 hours, 150 hours, and 174 hours, respectively.
- During the heat treatment, the average precipitate sizes does not change significantly.

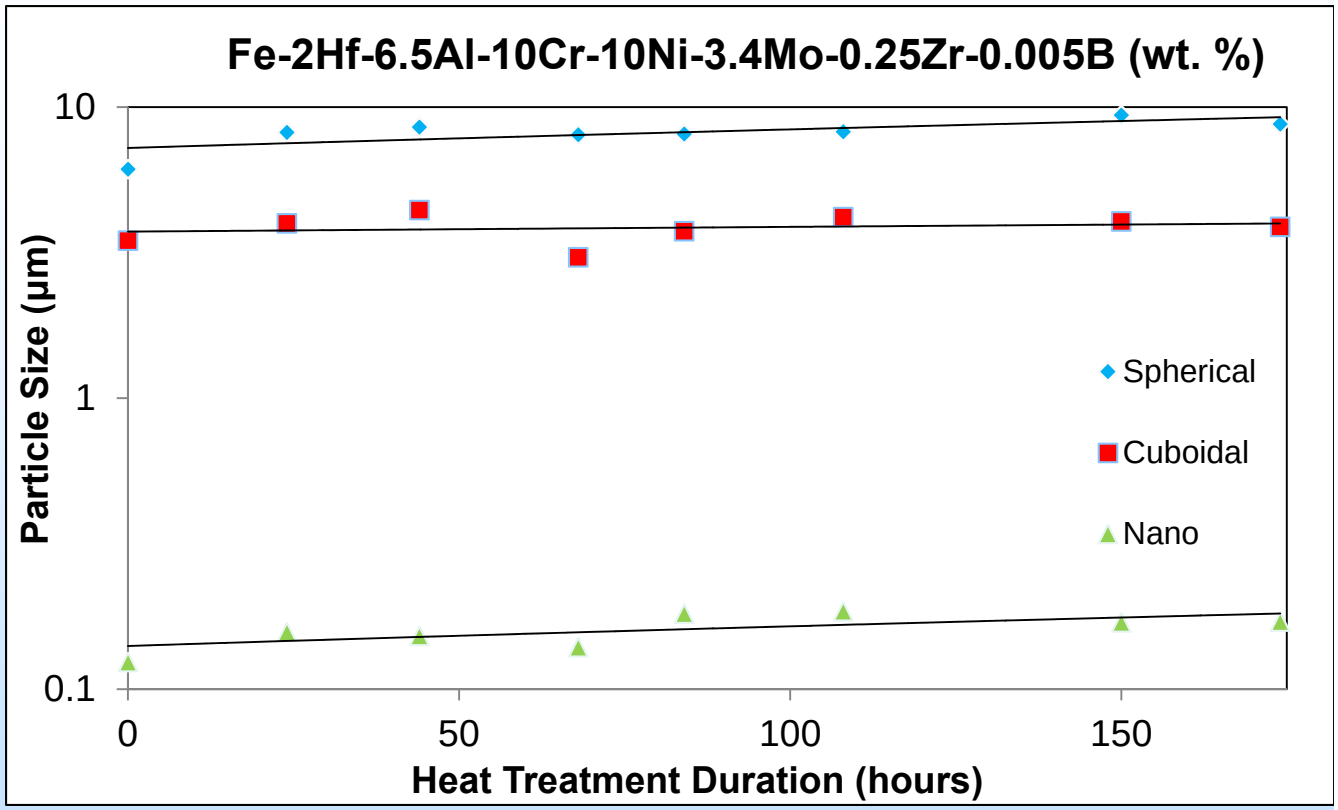

Aging Time (hrs)	0	24	44	68	84	108	150	174
Spherical	6.13	8.20	8.55	8.04	8.09	8.24	9.40	8.76
Cuboidal	3.48	3.99	4.43	3.05	3.75	4.19	4.05	3.88
Nano-sized	0.12	0.16	0.15	0.14	0.18	0.19	0.17	0.17

Neutron-Diffraction Experiments at Los Alamos Neutron Science Center (LANSCE)

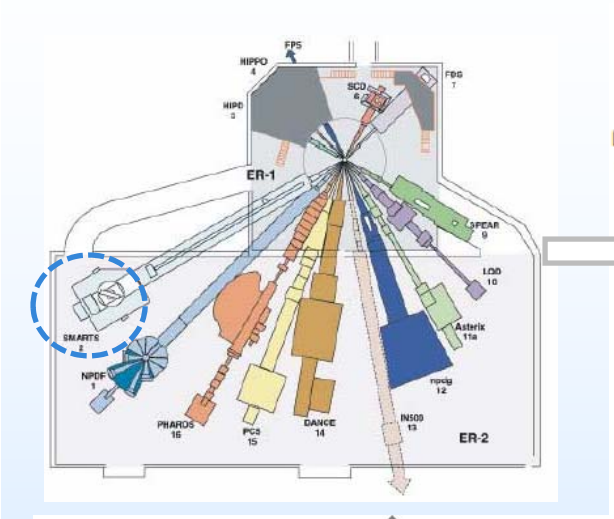

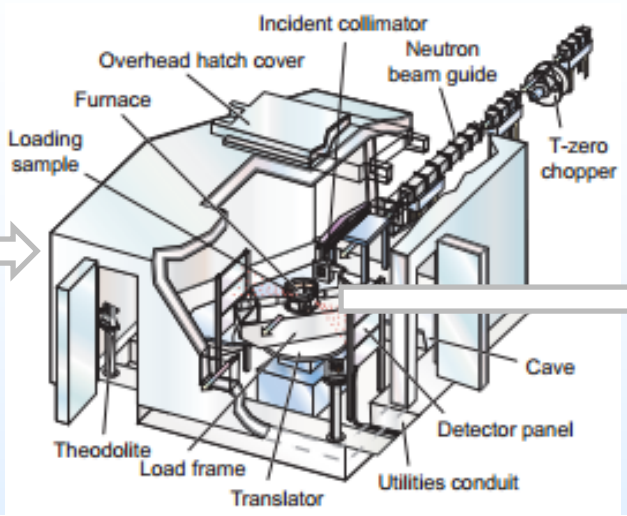

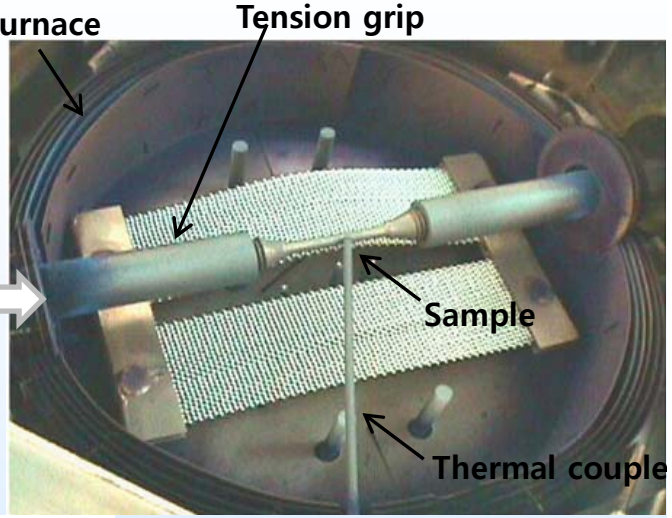

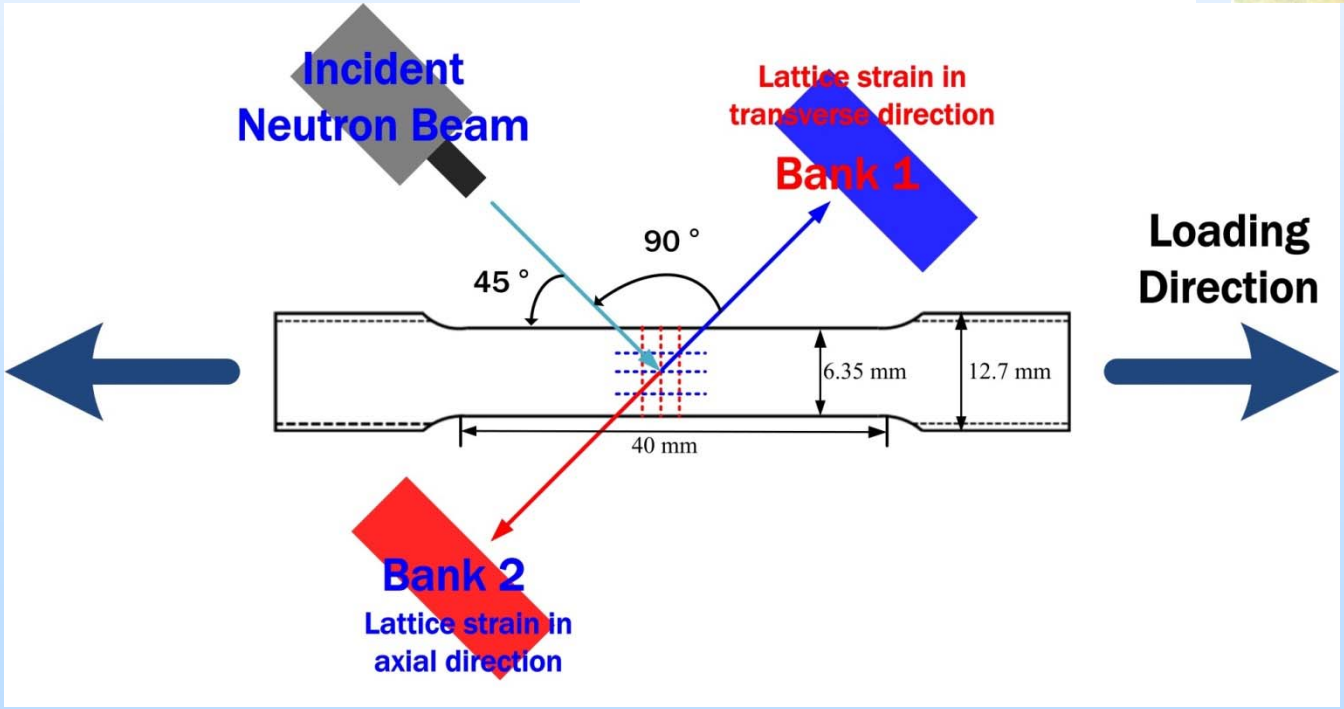

- The Spectrometer for MAterials Research at Temperature and Stress (SMARTS) at Los Alamos Neutron Science Center of the Los Alamos National Laboratory
- Measuring diffracted beams perpendicular and parallel to the loading direction, thus, transverse and axial lattice strains. temperatures

S. Huang, Y. Gao, K. An, L. Zheng, W. Wu, Z. Teng, P.K. Liaw, Acta Mater., 83, pp.137-148 (2015).

Elastic Strain Evolution during Loading

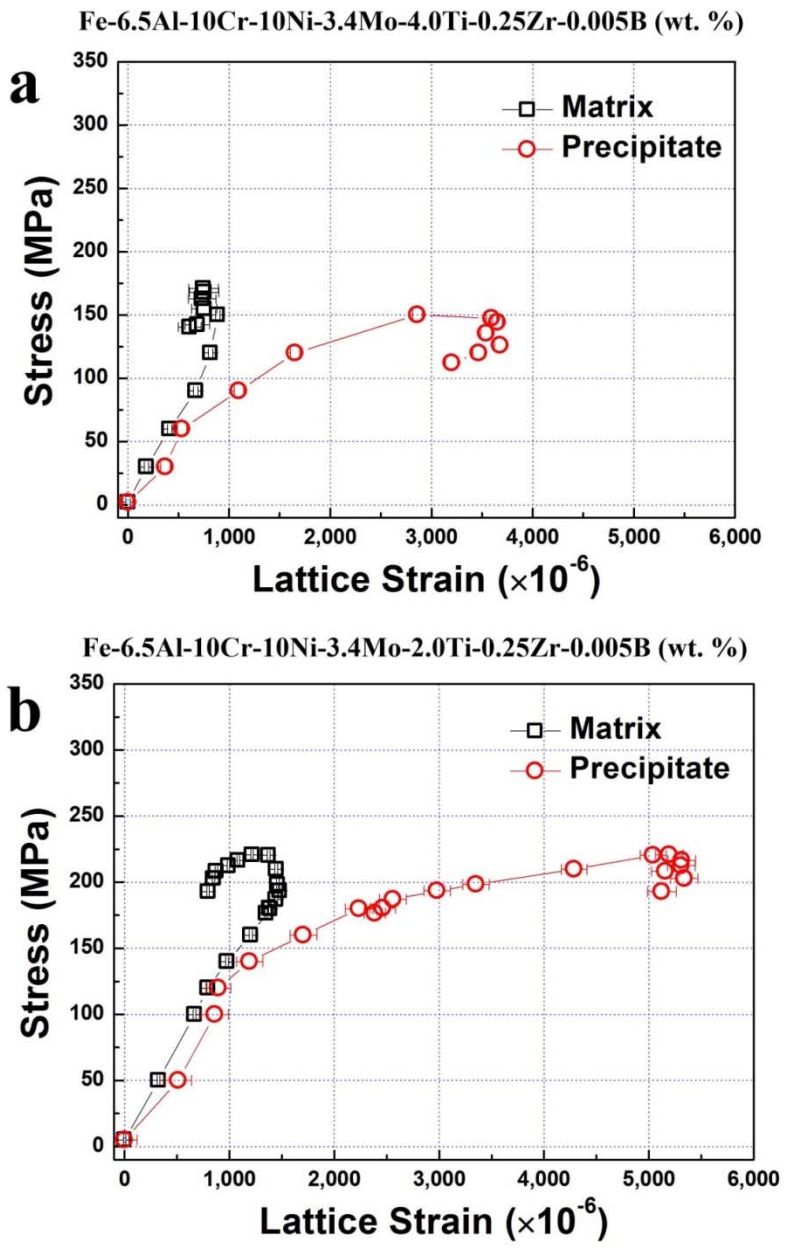

- Average phase strains along the axial direction at 973 K as a function of average stress during the in-situ tension experiments on (a) 4%-Ti alloy and (b) 2%-Ti alloy.
- The stress and lattice strain curves showed an elastic region and plastic region. The hooked section of the curve is the plastic region.
- The curves showed clear load transfer effect. After the matrix yields, the precipitates carry the load instead.
- 2%-Ti alloy has better load carry capability than 4%-Ti alloy, for its higher yield strength and larger lattice strain of the precipitate ($L2_1$/B2).

Gian Song, Zhiqian Sun, Lin Li, Bjørn Clausen, Shu Yan Zhang, Yanfei Gao, and Peter K. Liaw, Unpublished.

Crystal-Plasticity Finite-Element Model (CPFEM)

- **Prediction of elastic plastic response of lattice strain**
- **Comparison with experimental results**

Multiplicative decomposition

$$F = F^e F^p$$

$$F_{ij} = \partial x_i / \partial X_j = F^e_{ik} F^p_{kj}$$

elastic $T_{ij} = C_{ijkl} E^e_{kl}$

plastic $\dot{F}^p_{ik} F^{p-1}_{kj} = \sum_{\alpha=1}^{N_{SLIP}} \dot{\gamma}^{(\alpha)} s_i^{(\alpha)} m_j^{(\alpha)}$

Flow rule

$$\dot{\gamma}^\alpha = \dot{\gamma}^0 \left(\frac{\tau^\alpha}{g^\alpha} \right)^N$$

$$\tau^\alpha = m_i^\alpha F^{e-1}_{ij} J \sigma_{jk} F^e_{kl} s_l^\alpha$$

Hardening law

$$\dot{g}^\alpha = \sum_\beta h_{\alpha\beta} | \dot{\gamma}^\beta |$$

$$h_{\alpha\beta} = h_{\alpha\alpha} \left[q + (1-q) \delta_{\alpha\beta} \right]$$

$\dot{\gamma}^0$: characteristic strain rate

τ^α : resolved shear stress of α slip system

g^α : flow strength of α slip system

N : stress exponent

$h_{\alpha\beta}$: hardening moduli

$h_{\alpha\alpha}$: self-hardening moduli

q : latent hardening coefficient

h_0 : initia hardening modulus

τ_0 : initia slip strength

τ_s : saturation slip strength

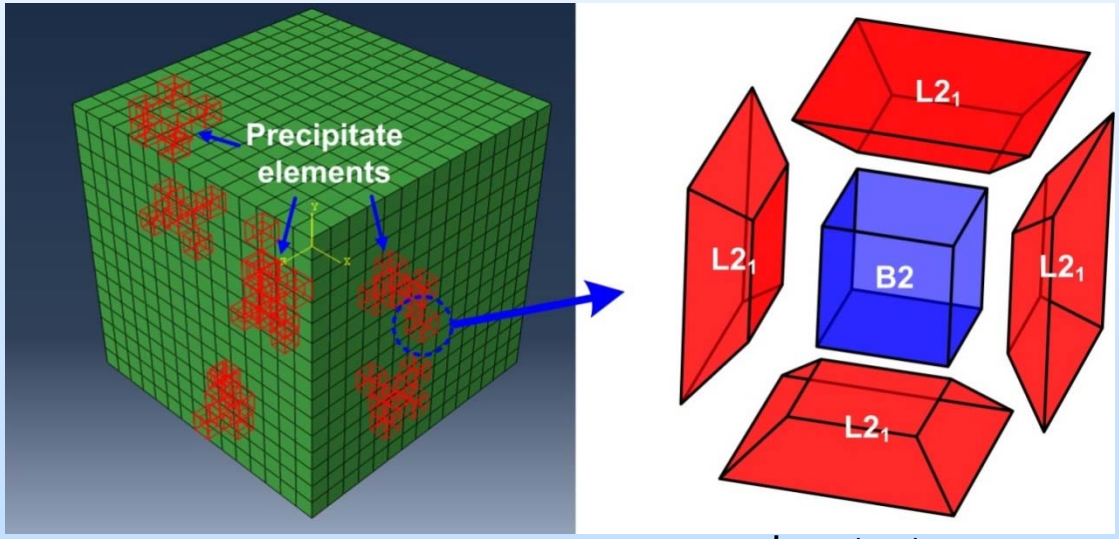

random texture

15 x 15 x 15 cubic model, Vol.% = ($L2_1$) 9.25 %, (B2) 9.25 %

(1) Peirce D, Asaro RJ, Needleman A. Acta Metallurgica 1982;30:1087.

(2) Bower AF, Wininger E. J. Mech. Phys. Solids 2004;52:1289.

(3) Zheng LL, Gao YF, Lee SY, Barabash RI, Lee JH, Liaw PK. J. Mech. Phys. Solids (2011), vol 59, p. 2307–2322

(4) Gian Song, Zhiqian Sun, Lin Li, Bjørn Clausen, Shu Yan Zhang, Yanfei Gao, and Peter K. Liaw, Unpublished.

Comparison Between ND results and Simulation

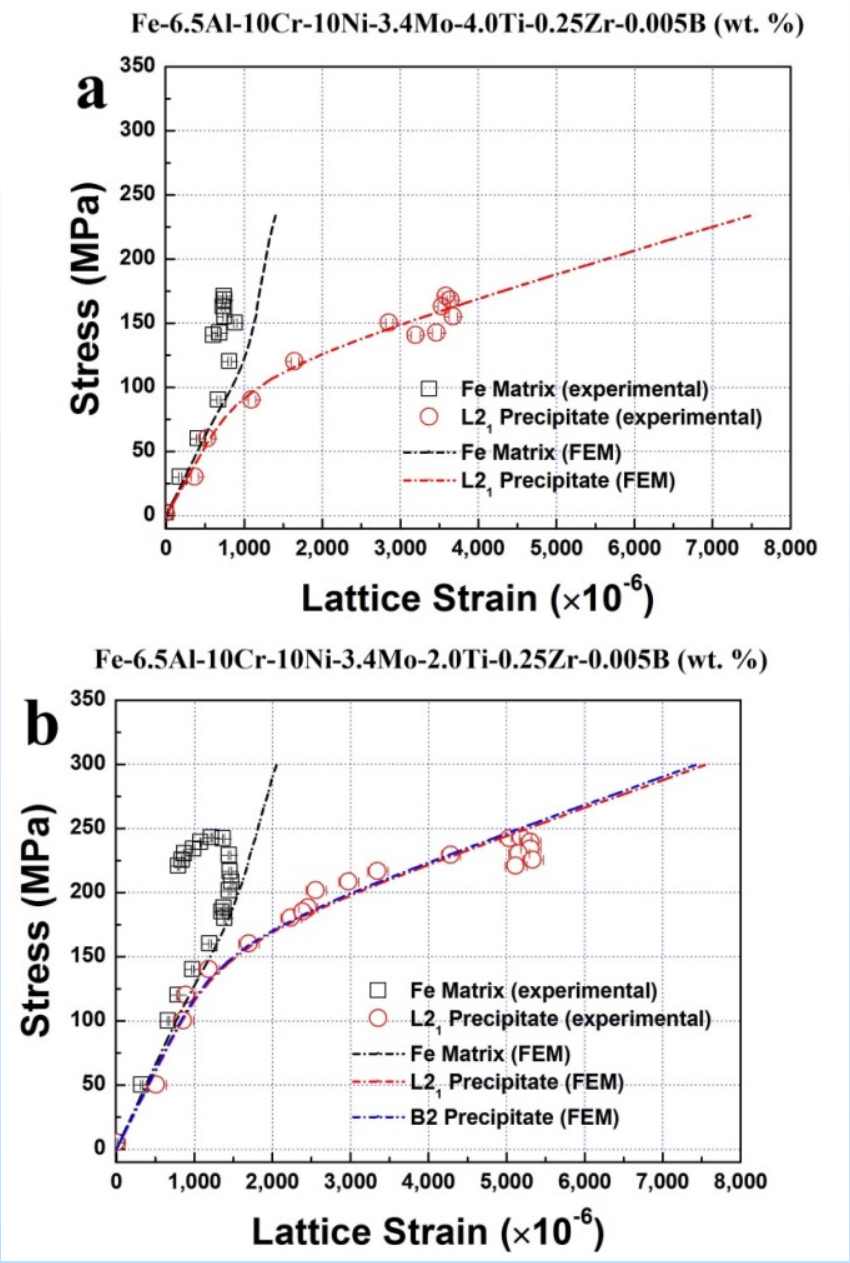

- In-situ neutron diffraction (ND) results and FEM simulation results comparison on the average phase strains along the axial direction at 973 K on (a) 4%-Ti alloy and (b) 2%-Ti alloy.
- The in-situ ND results and simulation results fit quite well in the elastic region.
- Discrepancy shown after the matrix yield, which is due to the strain-softening.

Gian Song, Zhiqian Sun, Lin Li, Bjørn Clausen, Shu Yan Zhang, Yanfei Gao, and Peter K. Liaw, Unpublished.

Calculations of Elastic Constants of Fe, *B*2, and $L2_1$ Phases

$$E(V,\{e_i\}) = E(V_0,0) - PV_0\sum_{i=1}^{3} e_i + \frac{V_0}{2}\sum_{i=1}^{6}\sum_{j=1}^{6} C_{ij}e_i e_j + O[e_i^3]$$

E: *internal energy*
e_i: *infinitesimal strain*
V_0: *volume of the unstrained crystal*
C_{ij}: *single-crystal elastic constants*
P: *pressure of the undistorted crystal at a volume, V_0*

		C_{ij} (GPa)		Expt.	Previous Calculations
		Energy-strain	Stress-strain		
Fe	C_{11}	264.37	288.73	243.1[1]	279[3]
	C_{12}	135.10	142.66	138.1[1]	140[3]
	C_{44}	91.21	91.76	121.9[1]	99[3]
B2-NiAl	C_{11}	207.30	208.44	206.7[2]	233[4], 236[5], 172.3[6]
	C_{12}	135.48	135.71	135.4[2]	173[4], 167[5], 146[6]
	C_{44}	116.18	117.20	116.8[2]	115[4], 140[5], 100.3[6]
$L2_1$-Ni_2TiAl	C_{11}	211.69	224.59	None	
	C_{12}	143.47	137.25		
	C_{44}	81.39	91.92		

1. J. Rayne, B. Chandrasekhar. Elastic constants of iron from 4.2 to 300 K, Physical Review 122, pp. 1714 (1961).
2. T. Davenport, L. Zhou, J. Trivisonno. Ultrasonic and atomic force studies of the martensitic transformation induced by temperature and uniaxial stress in NiAl alloys, Phys. Rev. B 59, p. 3421 (1999).
3. G. Guo, H. Wang. Gradient-corrected density functional calculation of elastic constants of Fe, Co and Ni in bcc, fcc and hcp structures, Chin. J. Phys 38, p. 949-961 (2000).
4. C. Fu, M. Yoo. Deformation behavior of B2 type aluminides: FeAl and NiAl, Acta metallurgica et materialia 40, p.703-711(1992) .
5. H. Fu, D. Li, F. Peng, T. Gao, X. Cheng. Ab initio calculations of elastic constants and thermodynamic properties of NiAl under high pressures, Computational Materials Science 44, p. 774-778 (2008).
6. J.F. Nye. Physical properties of crystals: their representation by tensors and matrices, Oxford university press, 1985.

Calculations of Orientation Dependence of Young's Modulus

$$\frac{1}{Y} = S_{11} - 2[(S_{11} - S_{12}) - \frac{1}{2}S_{44}](l_1^2 l_2^2 + l_2^2 l_3^2 + l_1^2 l_3^2)$$

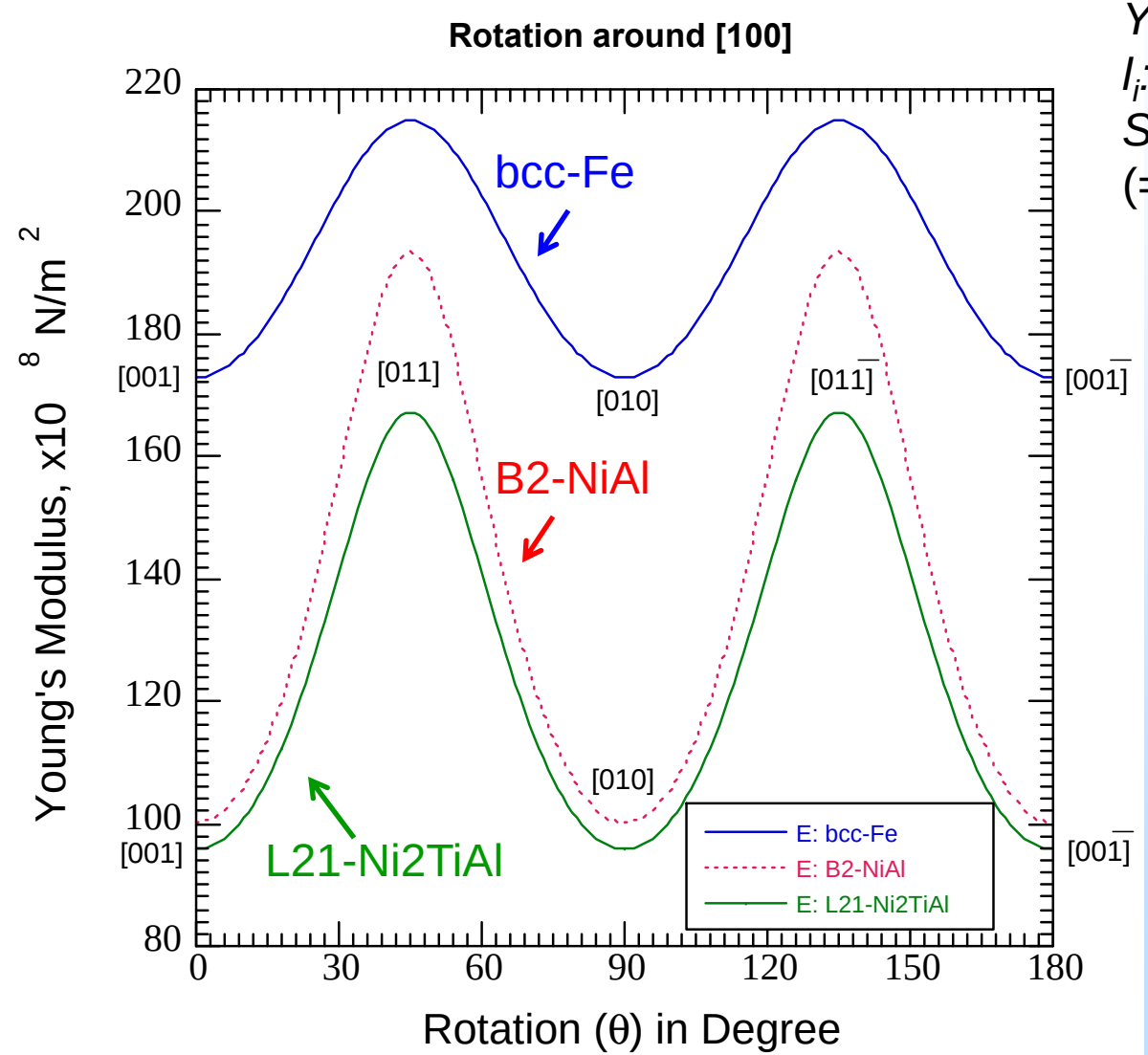

Y: Young's modulus
l_i: direction cosines
S_{ij}: elastic compliance constants (= C_{ij}^{-1})

The Young's modulus (E) in single-crystal (at 0 K) and its orientation dependence in bcc Fe, and B2-NiAl and $L2_1$-Ni_2TiAl phases, derived from calculated C_{ij} data. The tensile axis is rotated from [001] to [00$\bar{1}$], around [100], by 180 degrees.

Dislocation-dynamics simulations

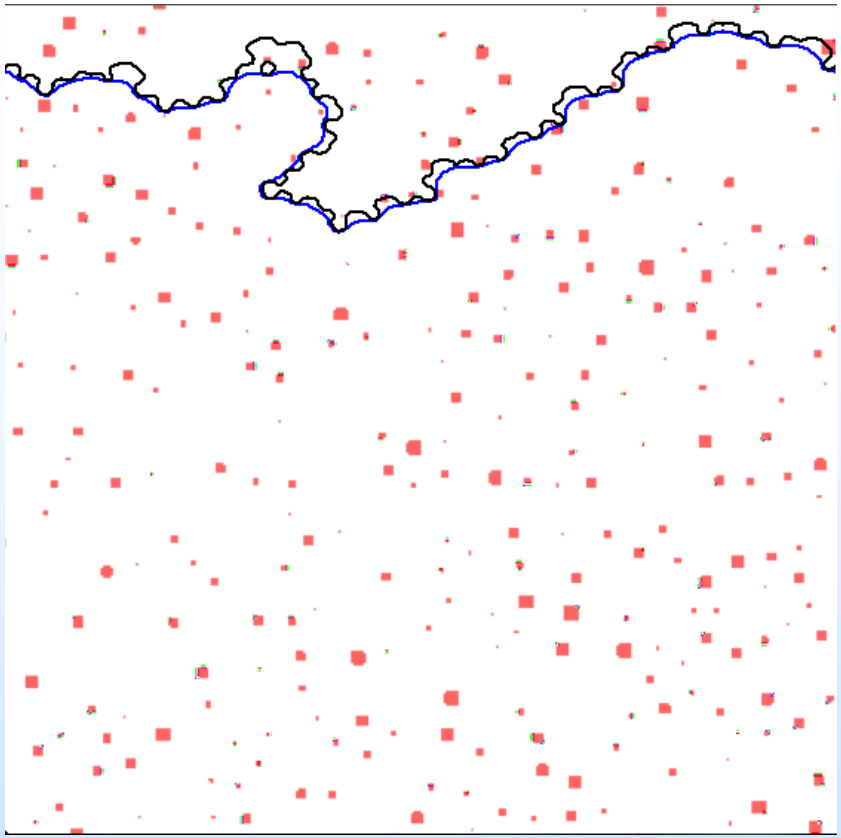

- **A three-dimensional field of close-packed precipitates with a given radius, volume fraction, and resistance to shear.**

- **Dislocations are placed in the glide plane, segmented, and stresses on each segment are calculated by solving the relevant force-balance equation for each segment:**

$$\tau_{ext} + \tau_{drag} + \tau_{obst} + \tau_{disloc} = 0$$

τ_{ext}: The force due to the externally-applied shear stress, the maximum value of which is taken as the predicted critical resolved shear stress (τ_{CRSS})on the glide plane.

τ_{drag}: The viscous drag force on a dislocation segment

τ_{obst}: The force from the stress field introduced by the precipitates

τ_{disloc}: The force on a given dislocation segment due to all other dislocation segments. (i.e., self-interaction)

V. Mohles, Materials Science and Engineering A 309, p. 265-269 (2001)

Dislocation-dynamics simulations (Cont'd)

Materials

•FBB8

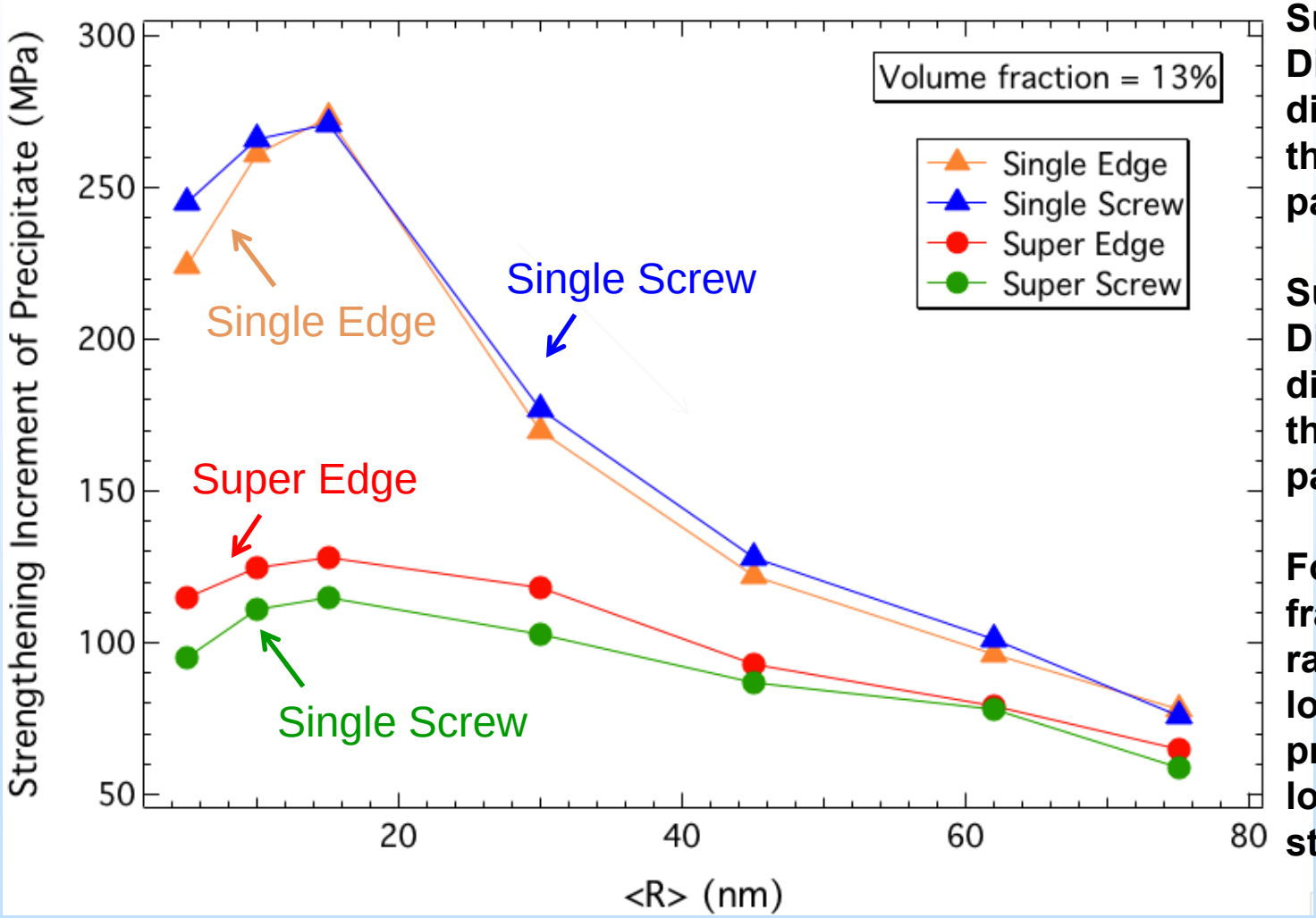

Super Edge Dislocation: Edge dislocation in alloys that composed of pair of dislocations.

Super Screw Dislocation: Screw dislocation in alloys that composed of pair of dislocations.

For a certain volume fraction, increase the radius of precipitates lower the number of precipitates, thus lower the strengthening effect.

Dislocation-dynamics simulation shows a much greater increase in the predicted stress for the single dislocation, as compared to the super-dislocation condition.

Dislocation-dynamics simulations (Cont'd)

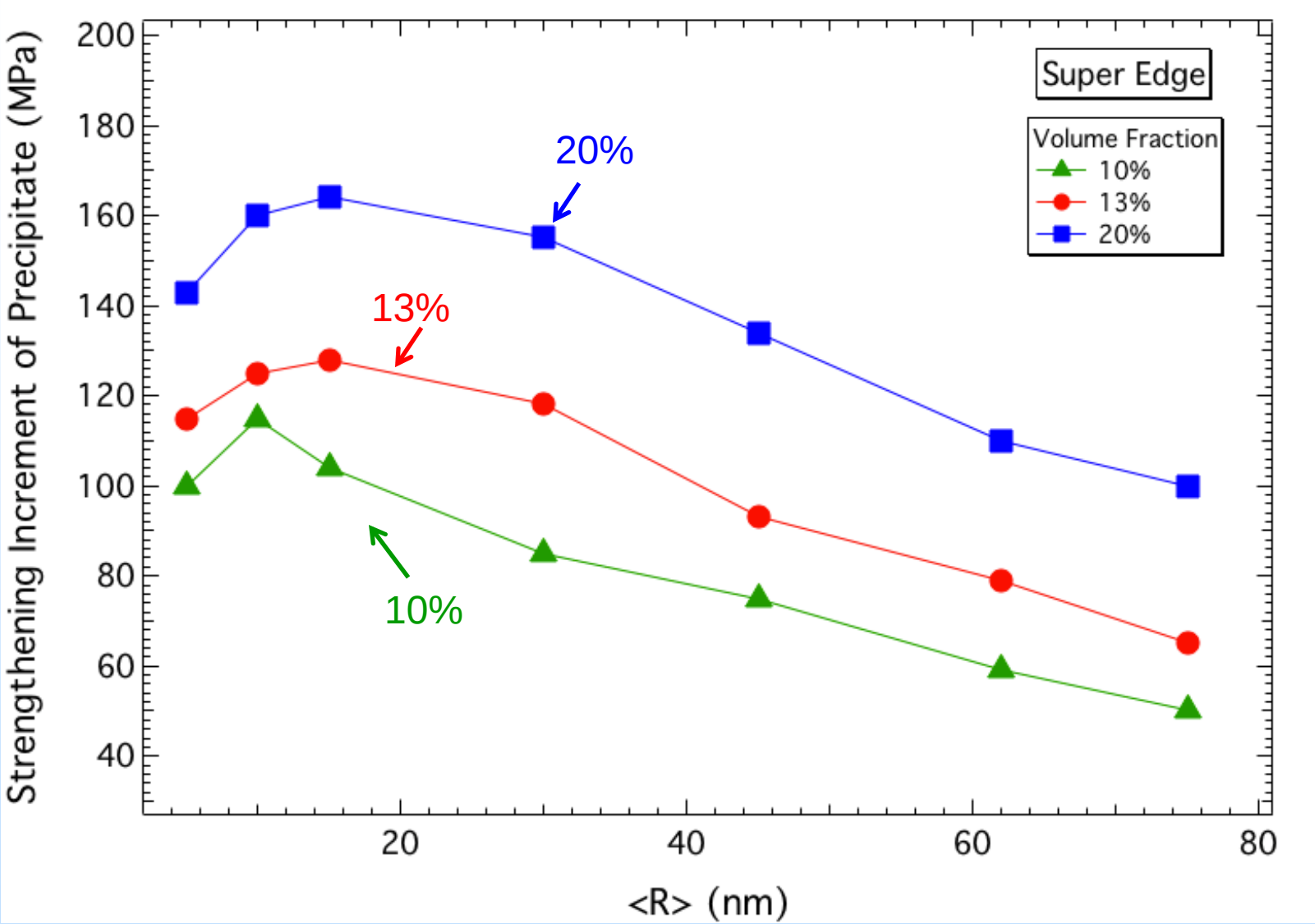

Dislocation-dynamics simulations (Cont'd)

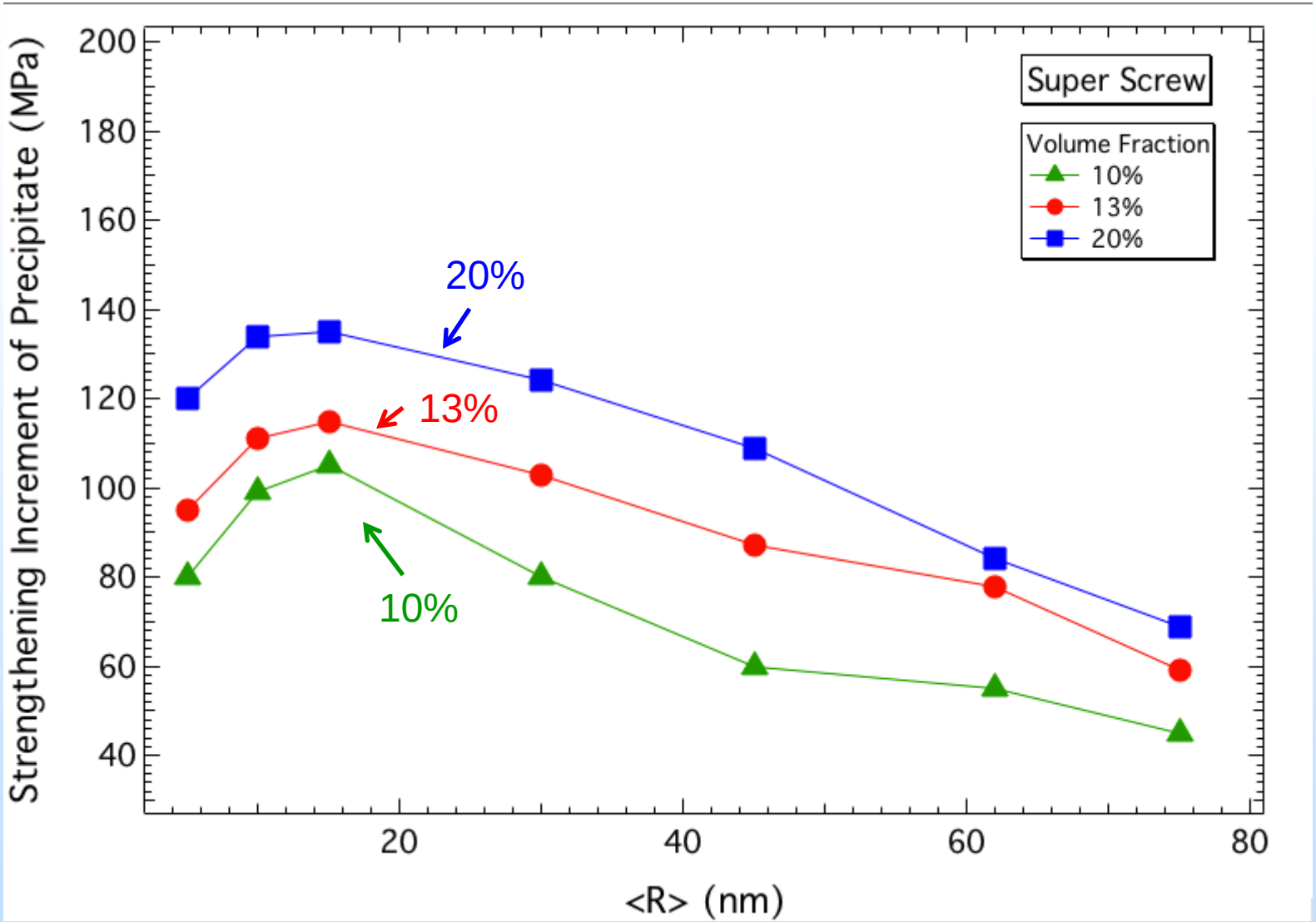

The increase in τ_p at small <r> values, and higher τ_p at higher volume fraction, show that the ideal microstructure is abundant of small precipitates.

Future Plans

Understanding and Optimization of Hierarchical-Precipitate-Strengthened Ferritic Alloys via Experimental and Computational Approaches

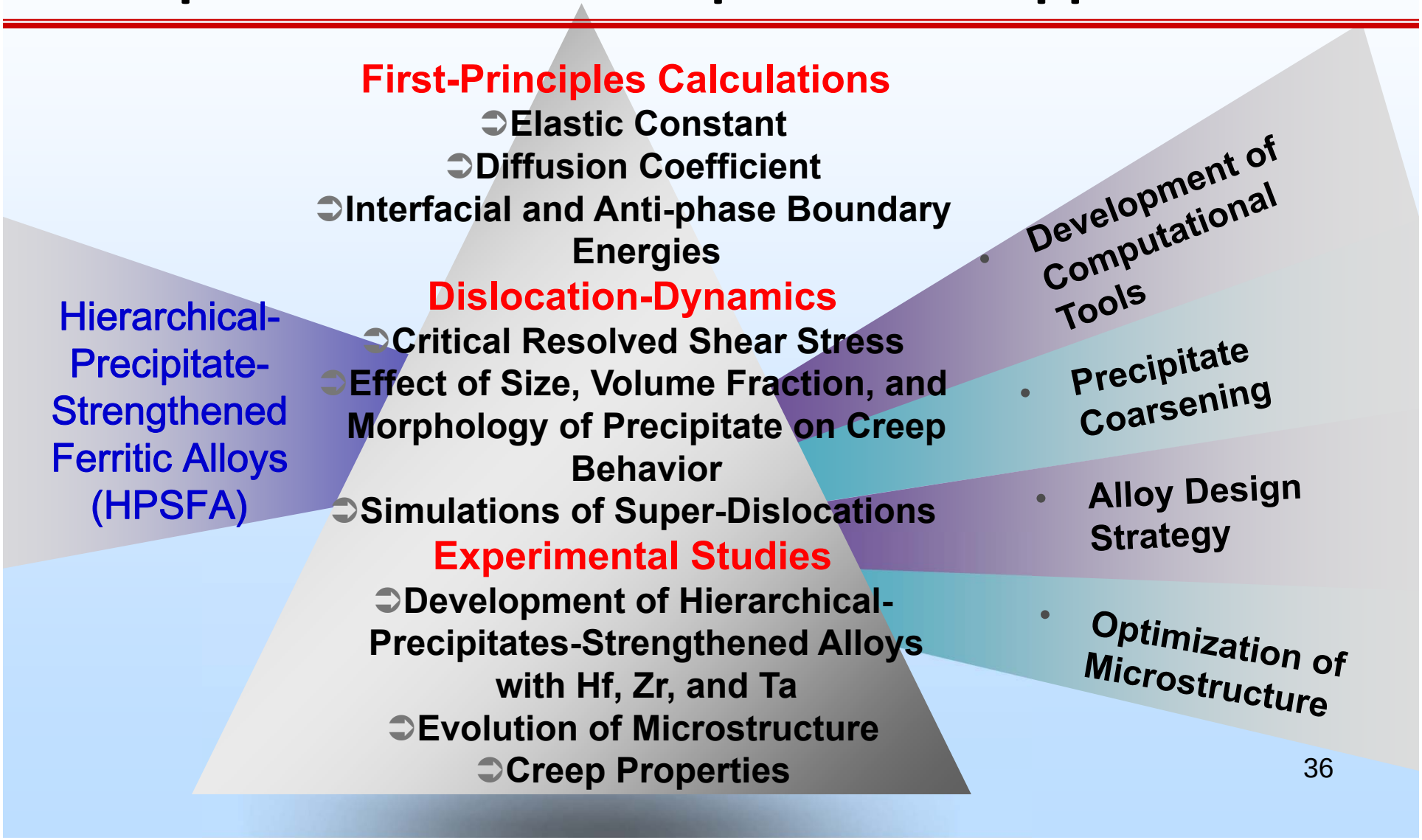

Conclusions

1. **First-Principles Calculations**
   - **Single-crystal elastic constants (C_{ij}) of $L2_1$ (Heusler) phases are calculated from first principles.**
   - **There is no experimental C_{ij} data of Heusler phases. Thus, calculations from first principles are the only viable option.**
2. **In-Situ Neutron-Creep Experiments on the 2%-Ti and 4%-Ti Alloys**
   - **The in-situ neutron-creep test on the 2%-Ti and 4%-Ti alloys at 973 K was performed at SMARTS located at the Los Alamos National Laboratory.**

Conclusions (Cont'd)

3. Microstructural Characterization

- It was found that the additions of 2% and 4% Ti into FBB8 was necessary to form the hierarchical ($L2_1$/B2) and single ($L2_1$) precipitate structure, which are super creep resistant at 973 K.
- SEM on the 2%-Hf alloy showed that undesirable precipitates formed instead of forming hierarchical structural precipitates, and TEM on the 1%-Hf-1%-Ti alloy showed that no B2/$L2_1$ hierarchical structural precipitates formed.
- Microstructural evolution for the 2%-Hf alloy has been investigated during the heat treatment. After 24 hours of heat treatment, the precipitate size remains stable.

Conclusions (Cont'd)

5. Ongoing Work and Future Plan

- First-principles calculations will be employed to derive the diffusion coefficients, and interfacial/anti-phase boundary energies.
- Current studies showed undesirable microstructures for 2%-Hf alloy, we will move to the research of 1%-Hf-1%-Ti alloy, and even 0.5%-Hf-1.5%Ti alloy.
- The effect of microstructure evolution on the creep behavior will be investigated by conducting creep tests on alloys with different precipitate structures (size and morphology).

Papers and Presentations

Papers

1) Z. K. Teng, M. K. Miller, G. Ghosh, C. T. Liu, S. Huang, K. F. Russel, M. E. Fine, and P. K. Liaw, Scripta Materialia, 2010;63:61.
2) S. Huang, D. L. Worthington, M. Asta, V. Ozolins, G. Ghosh, and P. K. Liaw, Acta Materialia, 2010;58:1982.
3) S. Huang, B. Clausen, D. Brown, Z. K. Teng, Y. F. Gao, and P. K. Liaw, Metallurgical and Materials Transactions A, 2012;43:1497.
4) Z. K. Teng, F. Zhang, M. K. Miller, C. T. Liu, S. Huang, Y. T. Chou, R. H. Tien, Y. A. Chang, and P. K. Liaw, Materials Letters, 2012;71:36.
5) Z. K. Teng, G. Ghosh, M. K. Miller, S. Huang, B. Clausen, D. W. Brown, and P. K. Liaw. Acta Mater. 2012;60:5362.
6) Z. K. Teng, C. T. Liu, M. K. Miller, G. Ghosh, E. A. Kenik, S. Huang, and P. K. Liaw, Materials Science and Engineering A, 2012;541:22.
7) H. Ding, S. Huang, G. Ghosh, P. K. Liaw, and M. Asta, Scripta Mater. 2012;67:732.
8) S. Huang, G. Ghosh, X. Li, J. Ilavsky, Z. K. Teng, and P. K. Liaw, Metallurgical and Materials Transactions A. 2012;43:3423.
9) C. H. Liebscher, V. Radmilovic, U. Dahmen, M. Asta and G. Ghosh, Journal of Materials Science,2013;48:2067.
10) Z. Sun, C. H. Liebscher, S. Huang, Z. Teng, G. Song, G. Wang, M. Asta, M. Rawlings, M. E. Fine, and P. K. Liaw, Scripta Materialia, 2013;68:384.

Papers and Presentations (Cont'd)

Papers (Cont'd)

11) H. Ding, V. I. Razumovsky, and M. Asta, Self Diffusion Anomaly in Ferromagnetic Metals: A Density-Functional-Theory Investigation of Magnetically Ordered and Disordered Fe and Co, Acta Mater., 70 (2014) 130-136.

12) H. Ding, V.I. Razumovskiy, M. Asta, Acta Mater., 70 (2014) 130-136.

13) S. Huang, Y. Gao, K. An, L. Zheng, W. Wu, Z. Teng, and P.K. Liaw, Acta Mater., 83 (2015) 137-148.

14) Z. Sun, G. Song, J. Ilavsky, and P.K. Liaw, Materials Research Letters, (2015) 128-134.

15) C.H. Liebscher, V.R. Radmilović, U. Dahmen, N.Q. Vo, D.C. Dunand, M. Asta, and G. Ghosh, Acta Mater., 92 (2015) 220-232.

16) G. Song, Z. Sun, L. Li, X. Xu, M. Rawlings, C.H. Liebscher, B. Clausen, J. Poplawsky, D.N. Leonard, S. Huang, Z. Teng, C.T. Liu, M.D. Asta, Y. Gao, D.C. Dunand, G. Ghosh, M. Chen, M.E. Fine, and P.K. Liaw, Ferritic alloy with extreme creep resistance via coherent hierarchical precipitates, Scientific Report, 5 (2015) 16327.

17) Z. Sun , G. Song , J. Ilavsky , G. Ghosh, and P.K. Liaw, Nano-sized precipitate stability and its controlling factors in a NiAl-strengthened ferritic alloy, Scientific Report, 5 (2015) 16081.

18) Z. Sun, G. Song, T. Sisneros, B. Clausen, C. Pu, L. Li, Y. Gao, and P. K. Liaw, Load Partitioning Between the BCC-Iron Matrix and Ni-Al-type Precipitates in a Ferritic Alloy on Multiple Length Scales, Scientific Reports 6 (2016) 23137

Papers and Presentations (Cont'd)

Presentations

1) Z. K. Teng, F. Zhang, M. K. Miller, C. T. Liu, A. Y. Chuang, S. Y. Huang, R. H. Tien, Y. T. Chou, and P. K. Liaw. 2011 TMS Meeting, San Diego, 02/27 – 03/04.
2) S. Y. Huang, B. Clausen, D. Brown, Z. Teng, G. Ghosh, M. Fine, and P. K. Liaw, 2011 TMS Meeting, San Diego, 02/27 – 03/04.
3) P. K. Liaw, Z. Teng, S. Huang, C. T. Liu, M. E. Fine, G. Ghosh, M. D. Asta, and G. Wang, The Annual University Coal Research/Historically Black Colleges and Universities and Other Minority Institutions Conference, Pittsburgh, Pennsylvania, 06/07 – 06/08, 2011
4) S. Huang, Y. F. Gao, K. An, W. Wu, L. Zheng, M. Rawlings, D. Dunand, and P. K. Liaw, 2012 TMS Meeting, Orlando, Florida , 03/11 – 03/15.
5) P. K. Liaw, M. D. Asta, D. C. Dunand, M. E. Fine, G. Ghosh, and C. T. Liu, National Energy Technology Laboratory, Pittsburgh, Pennsylvania, 04/18, 2012
6) C. H. Liebscher, V. Radmilovic, U. Dahmen, M. Asta, and G. Gosh, Microscopy & Microanalysis 2012 Meeting, Phoenix, Arizona, 07/29 - 08/02
7) C. H. Liebscher, V. Radmilovic, U. Dahmen, M. Asta, and G. Gosh, Materials Science and Technology 2012 Meeting, Pittsburgh, Pennsylvania, 08/07 - 08/11
8) H. Ding, S. Huang, G. Ghosh, P. K. Liaw, and M. Asta, Materials Science and Technology 2012 Meeting, Pittsburgh, Pennsylvania, 08/07 - 08/11
9) Z. Sun, G. Song, Z. Teng, G. Ghosh, and P. K. Liaw , 2012 MRS Fall Meeting & Exhibit, Boston, 11/25 – 11/30
10) P. K. Liaw, M. Asta, D, Dunand, M. Fine, G. Ghosh, C. Liu, H. Ding, S. Huang, M. Rawlings, Z. Sun, G. Song, Z. Teng, G. Wang, and C. Liebscher, 2013 TMS Meeting , San Antonio, Texas, 03/03 – 03/07

Papers and Presentations (Cont'd)

Presentations (Cont'd)

11) Z. Sun, S. Huang, Z. Teng, G. Song, G. Wang, and P. K. Liaw, 2013 TMS Meeting, San Antonio, Texas, 03/03 – 03/09

12) G. Song, Z. Sun, G. Wang, H. Ding, C. Liebscher, M. D. Asta, G. Ghosh, D. C. Dunand, M. Rawling, N. Q Vo, and P. K. Liaw, 2015 TMS Meeting, Orlando, Florida, 3/15 – 3/19

13) Z. Sun, G. Song, J. Ilavsky, and P. K. Liaw, 2015 Materials Science & Technology Conference (MS&T), Columbus, Ohio, 10/4 – 10/8

14) G. Song, Z. Sun, L. Li, X. Xu, M. Rawlings, C. Liebscher, B. Clausen, J. Poplawsky, D. Leonard, S. Huang, Z. Teng, C. Liu, M. Asta, Y. Gao, D. Dunand, G. Ghosh, M. Chen, M. Fine, and P. K. Liaw, 2015 Materials Science & Technology Conference (MS&T), Columbus, Ohio, 10/4 – 10/8

15) G. Song, Z. Sun, D. Dunand, M. Rawlings, G. Ghosh, and P. K. Liaw, 2016 TMS Meeting, Nashville, Tennessee, 02/14 – 02/18

16) G. Song, Y. Gao, Z. Sun, J. Poplawsky, and P. K. Liaw , 2016 TMS Meeting, Nashville, Tennessee, 02/14 – 02/18

17) Z. Sun, G. Song, J. Ilavsky, G. Ghosh, and P. K. Liaw, 2016 TMS Meeting, Nashville, Tennessee, 02/14 – 02/18

Awards

1) Zhiqian Sun, TMS Best Paper Contest – Graduate Division – First Place, TMS 2016 Annual Meeting & Exhibition, Feb. 14-18, 2016, Nashville, Tennessee
2) Gian Song, TMS Best Paper Contest – Graduate Division – Second Place, TMS 2016 Annual Meeting & Exhibition, Feb. 14-18, 2016, Nashville, Tennessee

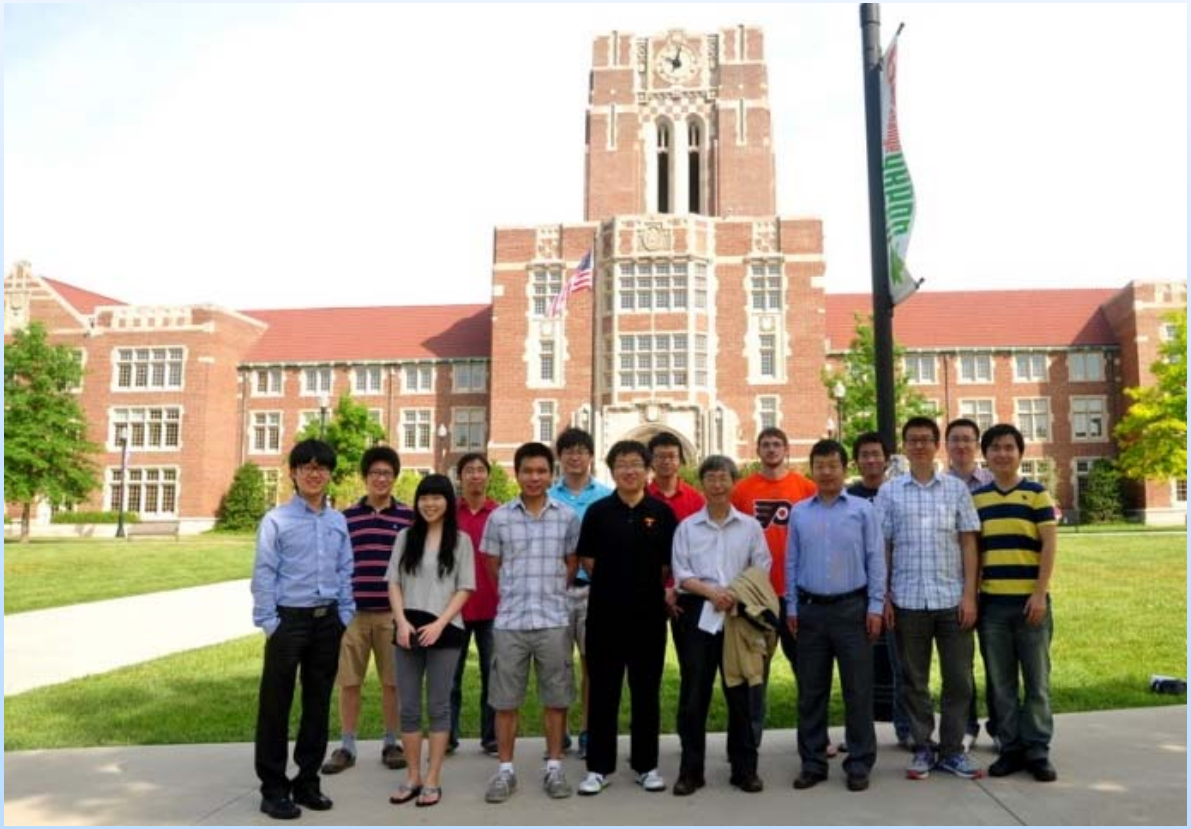

The TMS Award Ceremony, Nashville, Feb. 16, 2016

Zhiqian Sun with Dr. Patrice Turchi, the TMS Director

Gian Song with Dr. Patrice Turchi, the TMS Director

The TMS Award Ceremony, Nashville, Feb. 16, 2016

Zhiqian Sun (right), Prof. Liaw (center), and Gian Song (left) at the TMS award banquet.

Q & A

Thank you for your kind attention